Universidade Federal de Juiz de Fora

Programa de Pós-Graduação em Engenharia Elétrica

Engenharia Elétrica

Túlio Fernandes Moreira

# A Framework to unify HS-OFDM, OCDM, SCCP, and OSDM schemes under certain interference

Juiz de Fora

2022

Túlio Fernandes Moreira

# A Framework to unify HS-OFDM, OCDM, SCCP, and OSDM schemes under certain interference

Dissertação de mestrado apresentada ao Programa de Pós-Graduação em Engenharia Elétrica da Universidade Federal de Juiz de Fora, na area de concentração em sistemas eletrônicos, como requisito para obtenção do título de Mestre em Engenharia Elétrica.

Orientador: Prof. Dr. Moisés Vidal Ribeiro

Co-orientadora: Profa. Dra. Sobia Baig

Juiz de Fora

2022

Ficha catalográfica elaborada através do Modelo Latex do CDC da UFJF com os dados fornecidos pelo(a) autor(a)

Moreira, Túlio Fernandes.
A Framework to unify HS-OFDM, OCDM, SCCP, and OSDM schemes under certain interference / Túlio Fernandes Moreira. – 2022.
65 f. : il.

Orientador: Prof. Dr. Moisés Vidal Ribeiro
Co-orientadora: Profa. Dra. Sobia Baig
Dissertação de Mestrado – Universidade Federal de Juiz de Fora, Engenharia Elétrica. Programa de Pós-Graduação em Engenharia Elétrica, 2022.

1. Comunicação via rede de energia elétrica. 2. Modulação multiportadora. 3. Violação de comprimento de prefixo cíclico. 4. Deslocamento de tempo de símbolo.. I. Ribeiro, Moisés Vidal, orient. II. Baig, Sobia, coorient. III. Título

**FEDERAL UNIVERSITY OF JUIZ DE FORA**
**RESEARCH AND GRADUATE PROGRAMS OFFICE**

**Túlio Fernandes Moreira**

**A Framework to unify HS-OFDM, OCDM, SCCP, and OSDM schemes under certain interference**

Dissertation submitted to the Graduate Program in
Electrical Engineering of the Federal University of Juiz de Fora
as a partial requirement for obtaining a Master's degree
in Electrical Engineering. Concentration area: Electronic Systems

Approved on 14 of March of 2022.

**EXAMINING BOARD**

**Prof. Dr. Moisés Vidal Ribeiro –** Academic Advisor
Federal University of Juiz de Fora

**Prof. Dr. Sobia Baig**
COMSATS University Islamabad

**Prof. Dr. Luciano Manhães de Andrade Filho**
Federal University of Juiz de Fora

**Prof. Dr. Wallace Alves Martins**
Federal University of Rio de Janeiro

Juiz de Fora, 03/14/2022.

Documento assinado eletronicamente por **Moises Vidal Ribeiro**, **Professor(a)**, em 14/03/2022, às 11:51, conforme horário oficial de Brasília, com fundamento no § 3º do art. 4º do Decreto nº 10.543, de 13 de novembro de 2020.

Documento assinado eletronicamente por **Sobia Baig**, **Usuário Externo**, em 14/03/2022, às 11:53, conforme horário oficial de Brasília, com fundamento no § 3º do art. 4º do Decreto nº 10.543, de 13 de novembro de 2020.

Documento assinado eletronicamente por **Luciano Manhaes de Andrade Filho**, **Professor(a)**, em 14/03/2022, às 11:53, conforme horário oficial de Brasília, com fundamento no § 3º do art. 4º do Decreto nº 10.543, de 13 de novembro de 2020.

Documento assinado eletronicamente por **Wallace Alves Martins**, **Usuário Externo**, em 14/03/2022, às 11:54, conforme horário oficial de Brasília, com fundamento no § 3º do art. 4º do Decreto nº 10.543, de 13 de novembro de 2020.

A autenticidade deste documento pode ser conferida no Portal do SEI-Ufjf (www2.ufjf.br/SEI) através do ícone Conferência de Documentos, informando o código verificador **0700283** e o código CRC **93A0F604**.

*To my family*
*To my friends*
*To my advisors*
*To my colleagues*

## ACKNOWLEDGMENTS

Foremost, I thank God for giving me the strength to undertake this research study. I am thankful to my family, Sávio Fernandes Moreira, André Clemente Moreira, and Valéria Cristina Monteiro de Barros Fernandes, for giving me support and joyful moments throughout my life.

I also express my gratitude to my friends. They were always by my side and helped me relieve the pressure of my studies.

I would also like to thank LCOM's colleagues, especially Ândrei Camponogara and Mateus de Lima Filomeno, for their discussions on various subjects and continuous support and guidance throughout my master's studies.

I am also grateful to my advisors, Prof. Dr. Moisés Vidal Ribeiro and Profa. Dra. Sobia Baig, for all the support, positive criticism, and guidance of my work that helped me grow as a researcher.

I am also grateful to the thesis defense committee, composed of Prof. Dr. Luciano Manhães de Andrade Filho and Prof. Dr. Wallace Alves Martins, for evaluating my thesis and their valuable contributions.

Finally, I would like to thank all professors, employees, and colleagues at the Federal University of Juiz de Fora. They significantly contributed to my professional and personal training.

"If I have seen further, it is by standing upon the shoulders of giants"
Sir Isaac Newton

## RESUMO

A presente dissertação investiga os impactos das interferências causadas pela violação do comprimento de prefixo cíclico e deslocamento temporal de símbolo no desempenho de esquemas de comunicação de dados aplicados a transmissão de dados através da rede de energia elétrica (do inglês *power line communication* - PLC) quando vários esquemas de comunicação digital de dados são considerados. Nesse contexto, é introduzido um arcabouço capaz de unificar vários esquemas de comunicação de dados, que contêm transformação rápida de Fourier, quando os problemas supracitados são conjuntamente tratados. Baseando nesse arcabouço, expressões algébricas são apresentadas para os esquemas multiplexação ortogonal por divisão de chirp (do inglês *othogonal chirp division multiplexing* - OCDM), monoportadora com prefixo cíclico (do inglês *single carrier cyclic prefix* - SCCP) e multiplexação ortogonal por divisão de Stockwell (do inglês *orthogonal Stockwell division multiplexing* – OSDM). A partir dessas expressões algébricas, a presente dissertação mostra que os esquemas OCDM, SCCP e OSDM apresentam relações sinal-ruído normalizada (do inglês *normalized signal-to-noise ratio* - nSNR) igual à média harmônica da nSNR observada no esquema multiplexação por divisão de frequência ortogonal simétrica hermitiana (do inglês *hermitian symmetric orthogonal frequency division multiplexing* - HS-OFDM). Além disso, a capacidade do arcabouço em obter os esquemas HS-OFDM, OCDM, SCCP e OSDM a partir de uma mesma formulação facilita o projeto de transceptores que contemplem esses esquemas, os quais apresentam distintas vantagens e desvantagem em relação as características específicas dos meios de comunicação de dados. A presente dissertação também discute a análise numérica comparativa entre os esquemas HS-OFDM, OCDM, SCCP e OSDM para diferentes níveis de violações do comprimento prefixo cíclico e do deslocamento temporal de símbolo quando os canais de comunicação de dados são modelados como sistemas lineares e invariantes no tempo, ocupam a faixa de frequência entre 0 e 500 kHz e existe a presença aditiva de ruído modelado como processos aleatórios gaussiano branco e colorido. Os parâmetros balizadores da análise numérica comparativa é a taxa de bits, o que permite a alocação uniforme de potência (do inglês *uniform power allocation* - UA) e alocação ótima de potência (do inglês *optimal power allocation* - OA), e a probabilidade bits errados, a qual emprega a modulação digital adaptativa para alocar a mesma quantidade de bits nas subportadoras (HS-OFDM), subchips (OCDM), subsímbolos (SCCP) e grupos de subportadoras (OSDM). Considerando as informações dos estados do canal são completamente conhecidas pelo transmissor, a taxa de bits é utilizada como parâmetro de análise, enquanto a probabilidade de bits errados é utilizada como parâmetro de análise quando o transmissor não dispõe de nenhum conhecimento das informações dos estados do canal. Os resultados, em termos de taxa de bits, mostram que o HS-OFDM é o melhor esquema, seguido pelo OSDM. Já a análise, em termos de probabilidade de bits errados, mostra que o OCDM é o melhor esquema para lidar com a violação do comprimento do prefixo cíclico e deslocamento de tempo de símbolo. Finalmente, a presente dissertação mostra que a formulação unificada permite analisar

de forma comparativa vários esquemas de modulação digital de dados em diferentes cenários quando restrições e problemas distintos são considerados.

Palavras-chave: Comunicação via rede de energia elétrica, modulação multiportadora, violação de comprimento de prefixo cíclico, deslocamento de tempo de símbolo.

## ABSTRACT

This thesis investigates the impacts of interference caused by cyclic prefix (CP) violation and symbol timing offset (STO) in data communication schemes applied to power line communication (PLC) when different types of schemes are taken into account. In this context, it is presented a framework capable of unifying a set of data communication schemes, which uses the fast Fourier transform, when the aforementioned problems are considered. Based on the framework, closed-form equations are presented for the orthogonal chirp division multiplexing (OCDM), single carrier cyclic prefix (SCCP, and orthogonal Stockwell division multiplexing (OSDM). Relying on the derived expressions, this thesys shows that the OCDM, SCCP, and OSDM schemes present a normalized signal-to-noise ratio (nSNR) equal to the harmonic mean of the nSNR presented by the hermetian symmetric orthogonal frequency division multiplexing (HS-OFDM) scheme. Furthermore, the framework's ability to derive the HS-OFDM, OCDM, SCCP, and OSDM schemes from the same mathematical formulation facilitates the design of transceivers for those schemes, in which each of them presents diffenrents advantages and disadvanges in relation to specifics characteristics of the data communication media. This thesys also discusses the numerical analysis between the HS-OFDM, OCDM, SCCP, and OSDM for different levels of CP violation and STO when the data communication channels are modeled as linear and time invariant systems, which occupy the frequency width of 0 to 500 kHz and is disturbed by an additive noise modeled as white and colored Gaussian random process. The numerical analysis is based on the data rate, which allows uniform allocation (UA) and optimal allocation (OA), and bit error probability, which uses adaptative modulation to allocate the same amount of bits in each subcarrier (HS-OFDM), subchirp (OCDM), subsymbol (SCCP) and tile (OSDM). Considering that channel state information (CSI) is completely known by the transmitter, the main parameter for the analysis is the data rate. However, when CSI is not known at the transmitter side, the bit error probability is the main parameter. The data rate results show that HS-OFDM is the best scheme, followed by the OSDM, whilst the bit error probability results show the OCDM as the better one. Finally, the present thesis demonstrates that the unified mathematical formulation allows a comparative analysis of various data communication schemes when different scenarios with distinct problems are considered.



Key-words: Power line communication, multicarrier modulation, cyclic prefix length violation, symbol timing offset.

## LIST OF FIGURES

## LIST OF TABLES

## ACRONYMS

| | |
|---|---|
| **ACGN** | additive colored Gaussian noise |
| **AWGN** | additive white Gaussian noise |
| **BER** | bit error rate |
| **CDMA** | code-division multiple access |
| **CFR** | channel frequency response |
| **CIR** | channel impulse response |
| **CP** | cyclic prefix |
| **CSI** | channel state information |
| **CSS** | chirp spread spectrum |
| **C-ZF** | complete zero-forcing |
| **DFnT** | discrete Fresnel transform |
| **DFT** | discrete Fourier transform |
| **DOST** | discrete orthogonal Stockwell transform |
| **FDE** | frequency domain equalization |
| **FFT** | fast Fourier transform |
| **HS-OFDM** | Hermitian symmetric OFDM |
| **ICI** | inter-carrier interference |
| **ICpI** | inter-chirp interference |
| **IDFnT** | inverse discrete Fresnel transform |
| **IDFT** | inverse discrete Fourier transform |
| **IoT** | Internet of Things |
| **ISI** | inter-symbol interference |
| **IStI** | inter-slot interference |
| **ITI** | inter-tile interference |
| **MIMO** | multiple-input multiple-output |
| **M-ZF** | modified zero-forcing |
| **nSNR** | normalized signal-to-noise ratio |
| **OA** | optimal power allocation |
| **OCDM** | orthogonal chirp division multiplexing |
| **OFDM** | orthogonal frequency division multiplexing |

| | |
|---|---|
| **OTFDM** | orthogonal time-frequency division multiplexing |
| **OSDM** | orthogonal Stockwell division multiplexing |
| **PAM** | pulse amplitude modulation |
| **PHY** | Physical |
| **PLC** | power line communication |
| **PSD** | power spectral density |
| **QAM** | quadrature amplitude modulation |
| **SCCP** | single carrier cyclic prefix |
| **SINR** | signal-to-interference-plus-noise ratio |
| **SNR** | signal-to-noise ratio |
| **ST** | single-tap |
| **ST-ZF** | single-tap zero-forcing |
| **STO** | symbol timing offset |
| **UA** | uniform power allocation |
| **WSS** | wide-sense stationary |

**CONTENTS**

# 1 INTRODUCTION

The growing interest in PLC systems in the academic and industry sectors follows the ever-increasing demand for connectivity in modern society. In addition, it is being pushed forward by the necessity for developing pervasive telecommunication technologies and infrastructures for deploying smart grids, the Internet of Things (IoT), and Industry 4.0 solutions [1–5]. The primary motivation behind the research efforts toward PLC systems is the use of the already and widely deployed infrastructures of electric power systems as data communication media. However, electric power systems were conceived, specified, designed, and deployed for energy transmission using a significantly lower frequency than the frequencies used by narrowband and broadband PLC systems. In other words, electric power systems were not meant for data communication; consequently, they can impose substantial impairments on transmitting information-carrying signals with a high-frequency content. Several works point out the following impairments for using electric power systems as data communication media [6–13]: there are significant signal attenuation with the increase of the distance between transmitter and receiver and the frequencies used for data transmission at high rates; the presence of multi-path and frequency selectivity effects due to the occurrence of impedance mismatching along with the path between the transmitter and receiver; the presence of high-power impulsive noise related to switching behavior of electronics-based loads; time-varying characteristics of the data communication media due to the dynamics of loads and electric power systems; the presence of interference due to the use of electromagnetically unshielded power cables and operation in the the frequency bands in which wireless systems are primary users; the power cables degradation due to aging effects as time passes by; and restrictive constraints imposed by Telecommunication and Electricity Regulatory Authorities.

Surprisingly, the fact that PLC systems are quite old telecommunication technology, since the first efforts toward their development date back to the beginning of the XX century. Since then, bursts of development of PLC systems have been observed in different periods. The current burst of development started at the end of 90's of the XX century and has offered a deep understanding of the limitations and constraints of using electric power systems for data communication purposes in different scenarios and applications. Consequently, new PLC technologies have been introduced in the market due to academic and industrial efforts toward developing feasible protocols and standards. Despite the advances so far, there are still opportunities for fostering PLC systems because spectral efficiency, efficient energy consumption, flexibility, and spectral scarcity are driving research efforts to enlarge the usefulness of electric power systems as data communication media beyond the current stage of development. In this sense, research efforts for designing flexible and low energy consumption Physical (PHY) and link layers, full duplex communication, multiple-input multiple-output (MIMO) communication, energy harvesting, artificial intelligence, and combinations with other data communication media are being investigated. Regarding the PHY layer, it is well-established that the multicarrier scheme

known as orthogonal frequency division multiplexing (OFDM) is widely applied because it efficiently divides the available frequency band into several orthogonal subchannels. It is a useful feature for dealing with frequency selective channels to maximize data rate [14–21] or minimizing bit error rate (BER) in PLC and hybrid communication systems [22–25]. Moreover, the use of the single carrier cyclic prefix (SCCP) scheme was considered as an alternative to the OFDM by the authors in [26], showing that the SCCP achieves competitive BER performance in comparison to the OFDM when the normalized signal-to-noise ratio (nSNR) in the frequency domain is not frequency selective. Also, [27] analyzed a coded version of the SCCP scheme for PLC systems. Last but not least, the SCCP can also be implemented with the discrete Fourier transform (DFT).

Moreover, [28] proposed the orthogonal time-frequency division multiplexing (OTFDM), which can also be named as orthogonal Stockwell division multiplexing (OSDM)[1] scheme for reducing the computational complexity of the resource allocation process related to the bit and power allocations. The OSDM is based on the discrete orthogonal Stockwell transform (DOST) [29], which can be implemented using DFT [30, 31]. In the beginning, the DOST were mainly applied to digital image processing applications, such as image restoration, image compression, and face recognition [30, 32–34]. However, [28] showed that it can also be a useful multicarrier scheme in which the time-frequency region associated with only one OSDM symbol is divided into orthogonal tiles of distinct geometries. As each tile covers distinct time-frequency dimensions, the OSDM groups several contiguous subbands that show similar nSNR. As the OSDM was recently introduced, its performance analysis related to interference was not assessed. Similar to other multicarrier schemes, the performance of the OSDM can be seriously compromised when channel estimation, channel equalization, cyclic prefix (CP) length, symbol timing offset (STO), clock offset, and frequency offset[2] are not correctly handled.

The above discussion about SCCP and OSDM points out that the omnipresence of OFDM main not be mainly related to its characteristic of dealing with distinct types of channels. It is a well-established issue in the area of digital communication that what drives the use of OFDM is its fast implementation with the DFT. Another interesting scheme is the so-called orthogonal chirp division multiplexing (OCDM), introduced a few years ago. It relies on the combination of the orthogonality principle together with the chirp spread spectrum (CSS) scheme to yield a multichirp scheme. It was first proposed in [35] for passband data communication systems, and it was shown that the discrete Fresnel transform (DFnT), the main operation in the OCDM, can also be implemented using the DFT. Since then, a few researchers have advanced this scheme in other data communication media and applications. Investigations of OCDM in optical communications can be found in [36, 37], where it is shown that the coherent optical OCDM can be integrated into existing coherence optical OFDM. In MIMO systems, [38] pointed out

[1] This new name is suggested because it emphasizes characteristics that are shared with other well-known data communication schemes.

[2] The frequency offset problem emerges when performing passband data communication.

that the OCDM provides better performance than the OFDM in terms of BER. Also, [39, 40] analyzed the performance of the OCDM in underwater acoustic communication. Regarding the spectrum of the orthogonal chirps, [41] investigated its orthogonality in the discrete-time domain, while [42] proposed a shaping technique for it. Furthermore, [43, 44] applied OCDM in radar-communication and compared it with the OFDM for data communication and radar image generation; [44] also considered MIMO communication for radar systems. Moreover, [45] proposed a time-domain reflectometry system, based on the OCDM, for power line sensing. In addition, channel characterizations based on OCDM were conducted in [46], while [47] discussed a pilot signal for high precision characterization of channels. Finally, the literature has numerically shown that the OCDM scheme offers better BER performance than OFDM and SCCP schemes in a few circumstances. For instance, [48] showed such a result under the presence of frequency offset and narrowband interference. Paying attention to PLC systems, [49] extended the OCDM to operating the baseband and also compared them with the Hermitian symmetric OFDM (HS-OFDM) and SCCP under CP length violation; however, the underlying comparison was only supported by numerical simulations. No published study was found in the literature focusing on the sensitivity analysis of the baseband OCDM[3] concerning STO.

## 1.1 OBJECTIVES

Aiming to advance performance analyses when both the CP length violation and the STO are taken into account, and the combination of the schemes mentioned above for designing a flexible PHY layer of PLC systems, the following objectives are addressed in this thesis:

- To use the formulation discussed in [50, 51] for deriving closed-form expressions for quantifying the CP length violation and the STO in OCDM, SCCP, and OSDM schemes and performing a fair comparison among HS-OFDM, OCDM, SCCP, and OSDM under these problems when a baseband data communication through electric power systems are considered. Also, to present a framework for designing PLC systems that can easily choose between the HS-OFDM, OCDM, SCCP, or OSDM schemes for dealing with distinct scenarios when data communication through electric power systems is carried out.

- To numerically perform a comparison among HS-OFDM, OCDM, SCCP, and OSDM in terms of data rate and bit error probability under distinct levels of CP length violation and STO when the PLC channel is modeled as a linear and time-invariant system corrupted by the additive presence of random process, which is modeled as additive white Gaussian noise (AWGN) or additive colored Gaussian noise (ACGN). Furthermore, the data rate analysis covers the use of the uniform power allocation (UA) and optimal power allocation (OA) because they assume the availability of channel state information (CSI) at the

[3] In the rest of this dissertation, the acronym OCDM will refer to the baseband version of the OCDM.

transmitter side. In contrast, the bit error probability analysis only considers the lack of CSI at the transmitter side, which imposes the use of adaptive modulation.

## 1.2 ORGANIZATION

The remainder of this thesis is organized as follows:

- Chapter 2 addresses the problem formulation, which takes into account the system model of data communication schemes and the presence of CP length violation and STO. It also revisits the formulation for deriving the estimated signal, signal-to-interference-plus-noise ratio (SINR), signal-to-noise ratio (SNR), and nSNR of the HS-OFDM when the problems mentioned above are considered. Last but not least, it points out the research questions that this thesis aims to answer.
- Chapter 3 discusses a framework for allowing the easy exchange of HS-OFDM, OCDM, SCCP, and OSDM schemes in PLC systems when distinct channels conditions and constraints are considered. In the sequel, it extends the formulation in Chapter 2 for deriving the expressions for the estimated signal, SINR, SNR, and nSNR of the OCDM, SCCP, and OSDM schemes. Also, it pointed out the similarities between the data mentioned earlier communication schemes that support its easy exchange. Finally, it details a comparative discussion about the spectrogram and nSNR of these four data communication schemes.
- Chapter 4 analyzes the numerical results related to performance comparisons, in terms of data rate and error symbol probability, of the HS-OFDM, OCDM, SCCP, and OSDM schemes. The numerical results are obtained using closed-form expressions and Monte Carlo simulations.
- Chapter 5 discusses the main contributions of this thesis and future works.

# 2 PROBLEM FORMULATION

This chapter addresses the mathematical formulations for data communication schemes that use CP extension for imposing the channel convolutional matrix to be circulant[1], which relies on the assumption that the channel impulse response is linear and time-invariant, at least in a time period longer than the time duration associated with one $\tilde{N}$-length block. Also, it embraces the CP length violation and STO.

To derive a few closed-form expressions for such kinds of data communication schemes, a system model contemplating the HS-OFDM scheme under the presence of the CP length violation and STO is detailed. In the sequel, closed-form expressions for the received signal, SINR, and SNR are derived. The obtained mathematical formulation allows the performance analysis of data communication schemes due to the degradation yielded by CP length violation and STO.

This chapter is organized as follows: Section 2.1 presents the system model, Section 2.2 revisits the formulation found in [50, 51] for the HS-OFDM scheme for contemplating the degradation caused by CP length violation and STO, and formulates the investigated problem.

## 2.1 THE BASEBAND SYSTEM MODEL

Aiming to formulate the problem and point out the research questions investigated in this thesis, a vectorial version of the baseband PLC system model based on a data communication scheme in the discrete-time domain is shown in Figure 1. This data communication scheme which makes use of CP for ensuring the channel convolutional matrix is circulant and transmits $\tilde{N}$-block symbols of data. Note that $\tilde{N} = 2N + L_{cp}$, with $N$ being the number of samples of data in the transmitted block and $L_{cp}$ the CP length, which defines the redundant samples for ensuring the channel convolutional matrix is circulant as far as $L_{cp} \geq L_h - 1$, in which $L_h$ is the length of the time-invariant channel impulse response (CIR). It is assumed a lack of perfect synchronization at the receiver (i.e., STO) and the presence of inter-symbol interference (ISI) due to the violation of $L_{cp} \geq L_h - 1$, then the vectorial representation of the received $\tilde{N}$-block symbol in the discrete-time domain can be expressed as [50]

$$\mathbf{y}[l] = \sum_{i=-1}^{I} \mathbf{H}[-i]\mathbf{x}[l-i] + \mathbf{v}[l], \tag{2.1}$$

where $\mathbf{x}[l-i] = [x_0[l-i], \ldots, x_{\tilde{N}-1}[l-i]]^T \in \mathbb{R}^{\tilde{N}\times 1}$ is the $(l-i)^{th}$ $\tilde{N}$-block symbol transmitted; $-1 \leq i \leq I$, with $I = \lceil L_h/\tilde{N} \rceil$, $\lceil z \rceil = \min\{n \in \mathbb{Z} | n \geq z\}$ being the ceiling function, and $L_h$ being the channel length; and $\mathbf{v}[l] = [v_0[l], \ldots, v_{\tilde{N}-1}[l]]^T \in \mathbb{R}^{\tilde{N}\times 1}$ is the additive noise at the discrete time $l$, with $(\cdot)^T$ being the transpose operator. Moreover, $\mathbf{x}[l-i]$ and $\mathbf{v}[l]$ are independent

[1] If the channel convolutional matrix is circulant, then the discrete Fourier transform diagonalizes it. Consequently, discrete Fourier transform-based data communication scheme can be applied.

and zero mean wide-sense stationary (WSS) random vectors. Also, $\mathbf{H}[-i]$ is the CIR convolve matrix with entries equal to

$$H_{n,m}[-i] = \begin{cases} 0, & \mu + n - m < 0 \\ h_{\mu+n-m}, & 0 \leq \mu + n - m \leq L_h - 1 \\ 0, & L_h - 1 < \mu + n - m \end{cases}, \tag{2.2}$$

where $\mu = i\tilde{N} + \Delta$, in which $\Delta$ is the STO. In addition, $\mathbf{h} = [h_0, \ldots, h_{L_h-1}]^T \in \mathbb{R}^{L_h \times 1}$ is the vectorial representation of the CIR of the PLC channel, which is considered to be linear and time invariant. The time invariant assumption refers to the fact that the time interval for a $\tilde{N}$-block symbol is much shorter than the coherence time of the PLC channel. Further, it is defined the channel frequency response (CFR), $\boldsymbol{\mathcal{H}} = [\mathcal{H}_0, \ldots, \mathcal{H}_{2N-1}]^T$, with $\boldsymbol{\mathcal{H}} = \sqrt{2N}\mathbf{F}[\mathbf{h}^T \mathbf{0}^T_{(2N-L_h)\times 1}]^T$, where $\mathbf{F} \in \mathbb{C}^{2N \times 2N}$ is the normalized DFT matrix, $\mathbf{0}_{C\times D}$ is a $C \times D$-size matrix with entries equal to zero, and, finally, $\boldsymbol{\Lambda}_h = \text{diag}\{\boldsymbol{\mathcal{H}}\} \in \mathbb{C}^{2N\times 2N}$, with $\text{diag}\{\mathbf{z}\}$ representing a diagonal matrix containing the elements of the vector $\mathbf{z}$.

Figure 1 – The block diagram of the system model.

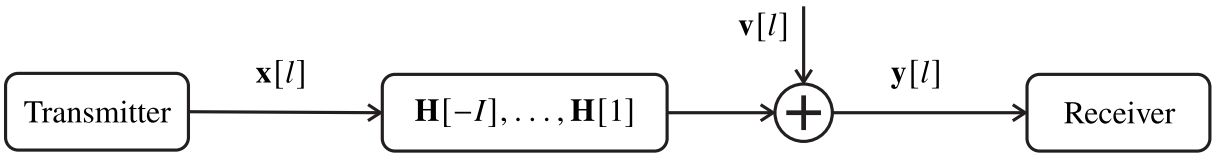


According to [50], (2.1) can be used to model the distortion introduced by the CP length violation and STO when the HS-OFDM scheme is used, see details in Section 2.2.

## 2.2 THE HS-OFDM SCHEME

This section revisits the mathematical formulation presented in [50] for quantifying the CP length violation and STO in the HS-OFDM scheme. In contrast to [50, 51], this thesis presents the mathematical derivations of a closed-form expression of the post-equalization SINR in the discrete-frequency domain, since it facilitates the recognition of the existing relationship with other data communication schemes addressed in Chapter 3.

In this regard, Figure 2 shows the block diagram for the HS-OFDM transmitter and receiver. At first, the vector representation of a modulated $N$-block symbol in the discrete-frequency domain, $\mathbf{X}[l] \in \mathbb{C}^{N\times 1}$, is mapped following the expression described by [14]

$$X_{\text{HS},k}[l] = \begin{cases} \Re\{X_{N-1}[l]\}, & k = 0 \\ X_{k-1}[l], & k = 1, \ldots, N-1 \\ \Im\{X_{N-1}[l]\}, & k = N \\ X^*_{\langle -k+1\rangle_{2N}}[l], & k = N+1, \ldots, 2N-1 \end{cases}, \tag{2.3}$$

Figure 2 – Block diagrams of the HS-OFDM's transmitter and receiver.

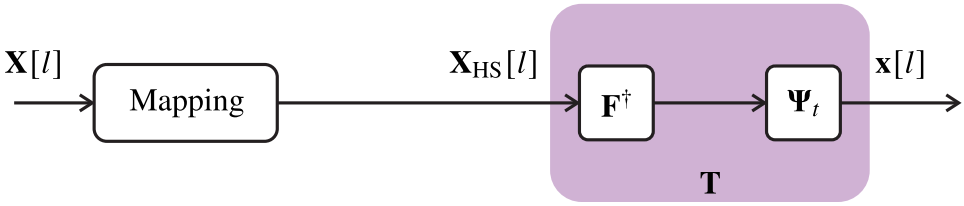


(a) Transmitter

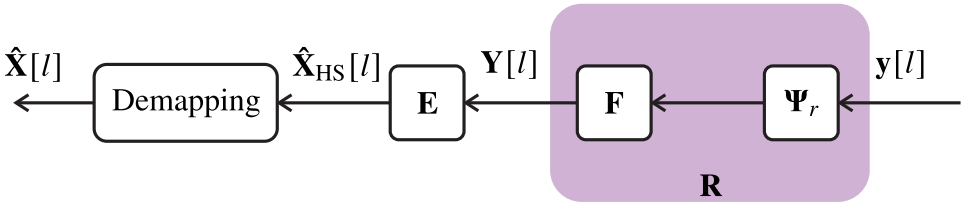


(b) Receiver

where $\langle\cdot\rangle_{2N}$ is the circular shift operation, $(\cdot)^*$ is the complex conjugate operator, $\Re\{\cdot\}$ and $\Im\{\cdot\}$ are the real and imaginary components of a complex value, respectively. Next, the vector representation of a $2N$-block modulated signal in the discrete-frequency domain, $\mathbf{X}_{\text{HS}} \in \mathbb{C}^{2N\times 1}$, is processed through the HS-OFDM transmitter by applying the normalized inverse discrete Fourier transform (IDFT) and then adding the CP. So, the vectorial representation of the $l^{th}$ $\tilde{N}$-block symbol at the output of the transmitter is given by

$$\begin{aligned}\mathbf{x}[l] &= \mathbf{T}\mathbf{X}_{\text{HS}}[l] \\ &= \mathbf{\Psi}_t\mathbf{F}^{\dagger}\mathbf{X}_{\text{HS}}[l],\end{aligned} \tag{2.4}$$

where $\mathbf{\Psi}_t$ is the CP matrix, which is expressed as

$$\mathbf{\Psi}_t = \begin{bmatrix} \mathbf{0}_{L_{cp}\times(2N-L_{cp})} & \mathbf{I}_{L_{cp}} \\ & \mathbf{I}_{2N} \end{bmatrix}, \tag{2.5}$$

in which $(\cdot)^{\dagger}$ is the Hermitian operator, $\mathbf{I}_{2N}$ and $\mathbf{I}_{L_{cp}}$ are the $2N \times 2N$ and $L_{cp} \times L_{cp}$ identity matrices, respectively. Therefore, the vectorial representation of the $l^{th}$ received $\tilde{N}$-block symbol is expressed as

$$\begin{aligned}\mathbf{y}[l] &= \sum_{i=-1}^{I} \mathbf{H}[-i]\mathbf{x}[l-i] + \mathbf{v}[l] \\ &= \sum_{i=-1}^{I} \mathbf{H}[-i]\mathbf{T}\mathbf{X}_{\text{HS}}[l-i] + \mathbf{v}[l].\end{aligned} \tag{2.6}$$

Considering $\mathbf{R} = \mathbf{F}\mathbf{\Psi}_r$, where $\mathbf{\Psi}_r$ is the remove CP matrix given by

$$\mathbf{\Psi}_r = [\mathbf{0}_{2N\times L_{cp}} \;\; \mathbf{I}_{2N}], \tag{2.7}$$

the vectorial representation of the $l^{th}$ $2N$-block symbol in the discrete-frequency domain is given by

$$\begin{aligned}\mathbf{Y}[l] &= \mathbf{R}\mathbf{y}[l] \\ &= \sum_{i=-1}^{I} \mathbf{RH}[-i]\mathbf{T}\mathbf{X}_{\mathrm{HS}}[l-i] + \mathbf{R}\mathbf{v}[l] \\ &= \mathbf{RH}[0]\mathbf{T}\mathbf{X}_{\mathrm{HS}}[l] + \sum_{\substack{i=-1 \\ i\neq 0}}^{I} \mathbf{RH}[-i]\mathbf{T}\mathbf{X}_{\mathrm{HS}}[l-i] + \mathbf{V}[l] \\ &= \mathbf{A}[0]\mathbf{X}_{\mathrm{HS}}[l] + \sum_{\substack{i=-1 \\ i\neq 0}}^{I} \mathbf{A}[i]\mathbf{X}_{\mathrm{HS}}[l-i] + \mathbf{V}[l],\end{aligned} \tag{2.8}$$

where $\mathbf{A}[i] = \mathbf{RH}[i]\mathbf{T}$ and $\mathbf{V}[l] = \mathbf{R}\mathbf{v}[l]$. Note that the CP length violation ($L_{cp} < L_h - 1$) and the presence of STO ($\Delta > 0$) are the causes of ISI and inter-carrier interference (ICI), respectively. To be more specific about the aforementioned interference, the following descriptions are made:

- ICI: Is the interference caused by others subcarriers from the $(l-i)^{th}$ $2N$-block symbols, $i = -1, 0, 1, \ldots, I$, into the desired subcarrier. The non-diagonal elements of $\mathbf{A}[i]$, $i = -1, 0, 1, \ldots, I$, contribute with this type of interference.
- ISI: Is the interference caused by the block signals $\mathbf{X}_{\mathrm{HS}}[l-i]$, $i = -1, 1, \ldots, I$, at the desired block signal $\mathbf{X}_{\mathrm{HS}}[l]$. The diagonal elements of $\mathbf{A}[i]$, $i = -1, 1, \ldots, I$, contribute with this type of interference.

Regarding the equalization process in the discrete-frequency domain, one can straightforwardly use the complete zero-forcing (C-ZF) equalizer, that mitigates ISI and ICI caused by the channel, CP length violation and the STO. A second option is to use the modified zero-forcing (M-ZF) equalizer, which mitigates the ISI caused by the channel and the ICI. Or, as a third option, the single-tap zero-forcing (ST-ZF) equalizer that addresses ISI caused by the channel, see [51] for more details. To put in mathematical terms, these equalizers are given by

$$\mathbf{E} = \begin{cases} \mathbf{A}^{\dagger}[0]\left(\sum_{i=-1}^{I} \mathbf{A}^{\dagger}[i]\mathbf{A}[i]\right)^{-1} & \text{for C-ZF} \\ (\mathbf{A}^{\dagger}[0]\mathbf{A}[0])^{-1}\mathbf{A}^{\dagger}[0] & \text{for M-ZF} \\ (\mathcal{D}\{\mathbf{A}[0]\})^{-1} & \text{for ST-ZF} \end{cases}, \tag{2.9}$$

where $\mathcal{D}\{\mathbf{Z}\}$ represents a diagonal matrix containing the diagonal elements of the matrix $\mathbf{Z}$. Therefore, the vectorial representation of an estimate of the received $l^{th}$ $2N$-block symbol, before

the demapping process, is given by,

$$\begin{aligned}\hat{\mathbf{X}}_{\mathrm{HS}}[l] &= \mathbf{EA}[0]\mathbf{X}_{\mathrm{HS}}[l] + \sum_{\substack{i=-1 \\ i\neq 0}}^{I} \mathbf{EA}[i]\mathbf{X}_{\mathrm{HS}}[l-i] + \mathbf{EV}[l] \\ &= \mathcal{D}\{\mathbf{EA}[0]\}\mathbf{X}_{\mathrm{HS}}[l] + \overline{\mathcal{D}}\{\mathbf{EA}[0]\}\mathbf{X}_{\mathrm{HS}}[l] + \sum_{\substack{i=-1 \\ i\neq 0}}^{I} \mathbf{EA}[i]\mathbf{X}_{\mathrm{HS}}[l-i] + \mathbf{EV}[l],\end{aligned} \tag{2.10}$$

in which $\overline{\mathcal{D}}\{\mathbf{Z}\} = \mathbf{Z} - \mathcal{D}\{\mathbf{Z}\}$. However, the interference that disturbs the data communication is avoidable when the correct value of $L_{cp}$ and the absence of STO apply. To put in mathematical terms:

- If $L_{cp} > L_h - 1$ is adopted, then $\mathbf{A}[i] = \mathbf{0}_{2N}$ for $i = 1, \ldots, I$.
- If $\Delta = 0$ is adopted, then $\mathbf{A}[-1] = \mathbf{0}_{2N}$.
- If the two above conditions are taken into account, then $\mathbf{A}[0]$ will be a diagonal matrix with elements equal to the CFR, meaning $\mathbf{A}[0] = \mathbf{\Lambda}_h$. Also, the equalizer $\mathbf{E}$ will result into the single-tap (ST) equalizer $\mathbf{E} = \mathbf{\Lambda}_h^{-1}$.

Therefore, if the last condition is adopted, the only disturbance left in the $l^{th}$ estimated $2N$-block symbol is caused by the additive noise $\mathbf{V}[l]$. Consequently, (2.10) reduces to

$$\hat{\mathbf{X}}_{\mathrm{HS}}[l] = \mathbf{X}_{\mathrm{HS}}[l] + \mathbf{\Lambda}_h^{-1}\mathbf{V}[l]. \tag{2.11}$$

Finally, the last step in the HS-OFDM reception is the demapping yielding $\hat{\mathbf{X}}[l]$, whose elements are equal to

$$\hat{X}_k[l] = \begin{cases} \hat{X}_{\mathrm{HS},k+1}[l], & k = 0, \ldots, N-2 \\ \hat{X}_{\mathrm{HS},0}[l] + j\hat{X}_{\mathrm{HS},N-1}[l], & k = N-1 \end{cases}. \tag{2.12}$$

Now, the SINR analysis for the HS-OFDM scheme is presented. The mathematical deductions of SINR is carried out after the discrete-frequency domain equalization, which is slight different from the approach presented in [50], in which the deduction of SINR is carried out before the frequency domain equalization process. The choice in favor of the deduction of SINR after the frequency domain equalization (FDE) facilitates the comparison between HS-OFDM and the other schemes (i.e., SCCP, OSDM, and OCDM) as will be clear in Chapter 3. In this sense, the following components can be identified in (2.10):

- $\mathcal{D}\{\mathbf{EA}[0]\}\mathbf{X}_{\mathrm{HS}}[l]$ as the desired signal.
- $\overline{\mathcal{D}}\{\mathbf{EA}[0]\}\mathbf{X}_{\mathrm{HS}}[l] + \sum_{\substack{i=-1 \\ i\neq 0}}^{I} \mathbf{EA}[i]\mathbf{X}_{\mathrm{HS}}[l-i]$ as summation of ISI and ICI.
- $\mathbf{EV}[l]$ as the additive noise.

Therefore, the desired signal power matrix is defined as

$$\begin{aligned}\boldsymbol{\mathcal{P}}_{\mathbf{S}} &= \frac{1}{2N}\mathcal{D}\{\mathbf{EA}[0]\}\mathbb{E}\{\mathbf{X}_{\mathrm{HS}}[l]\mathbf{X}_{\mathrm{HS}}^{\dagger}[l]\}\mathcal{D}\{\mathbf{EA}[0]\}^{\dagger} \\ &= \mathcal{D}\{\mathbf{EA}[0]\}\boldsymbol{\mathcal{P}}_{\mathbf{X}}\mathcal{D}\{\mathbf{EA}[0]\}^{\dagger}\end{aligned} \tag{2.13}$$

while the interference-plus-noise power matrix is equal to

$$\begin{aligned}\boldsymbol{\mathcal{P}}_{\mathbf{IV}} = &\frac{1}{2N}\overline{\mathcal{D}}\{\mathbf{EA}[0]\}\mathbb{E}\{\mathbf{X}_{\mathrm{HS}}[l]\mathbf{X}_{\mathrm{HS}}^{\dagger}[l]\}\overline{\mathcal{D}}\{\mathbf{EA}[0]]\}^{\dagger}+ \\ &\frac{1}{2N}\sum_{\substack{i=-1\\ i\neq 0}}^{I}\mathbf{EA}[i]]\mathbb{E}\{\mathbf{X}_{\mathrm{HS}}[l-i]\mathbf{X}_{\mathrm{HS}}^{\dagger}[l-i]\}\mathbf{A}^{\dagger}[i]\mathbf{E}^{\dagger}+\frac{1}{2N}\mathbf{E}\mathbb{E}\{\mathbf{V}[l]\mathbf{V}^{\dagger}[l]\}\mathbf{E}^{\dagger} \\ = &\overline{\mathcal{D}}\{\mathbf{EA}[0]\}\boldsymbol{\mathcal{P}}_{\mathbf{X}}\overline{\mathcal{D}}\{\mathbf{EA}[0]\}^{\dagger}+\sum_{\substack{i=-1\\ i\neq 0}}^{I}\mathbf{EA}[i]\boldsymbol{\mathcal{P}}_{\mathbf{X}}\mathbf{A}^{\dagger}[i]\mathbf{E}^{\dagger}+\mathbf{E}\boldsymbol{\mathcal{P}}_{\mathbf{V}}\mathbf{E}^{\dagger}\end{aligned} \tag{2.14}$$

with $\boldsymbol{\mathcal{P}}_{\boldsymbol{V}} = \frac{1}{2N}\mathbb{E}\{\mathbf{V}[l]\mathbf{V}^{\dagger}[l]\} \in \mathbb{R}^{2N\times 2N}$ and $\mathbb{E}\{\cdot\}$ being the expectation operator. Note that $\boldsymbol{\mathcal{P}}_{\mathbf{X}}$ and $\boldsymbol{\mathcal{P}}_{\boldsymbol{V}}$ are diagonal matrices because the elements of $\mathbf{X}_{\mathrm{HS}}[l]$ and $\mathbf{V}[l]$ are obtained from mean zero WSS random processes, which are constituted by uncorrelated samples.

Finally, the SINR for the $k^{\mathrm{th}}$ subcarrier is given by

$$\gamma_{\mathrm{IV},k} = \frac{\mathcal{P}_{\mathrm{S},k,k}}{\mathcal{P}_{\mathrm{IV},k,k}}, \tag{2.15}$$

where $\mathcal{P}_{\mathrm{X},k,k}$ and $\mathcal{P}_{\mathrm{IV},k,k}$ are the $k^{\mathrm{th}}$ diagonal element of $\boldsymbol{\mathcal{P}}_{\mathbf{X}}$ and $\boldsymbol{\mathcal{P}}_{\mathbf{IV}}$, respectively. In the case without interference (i.e., $L_{cp} \geq L_h - 1$ and $\Delta = 0$), from (2.11) it is extracted the expression of the mapped estimated signal in the $k^{th}$ subcarrier of the $l^{th}$ $2N$-block symbol, which is given by

$$\hat{X}_{\mathrm{HS},k}[l] = X_{\mathrm{HS},k}[l] + \Lambda_{h,k,k}^{-1}V_k[l], \tag{2.16}$$

where $\Lambda_{h,k,k}$ is the $k^{th}$ diagonal element of $\boldsymbol{\Lambda}_h$. So, the SNR of the $k^{\mathrm{th}}$ subcarrier is equal to

$$\begin{aligned}\gamma_{\mathrm{V},k} &= \frac{\frac{1}{2N}\mathbb{E}\{X_{\mathrm{HS},k}[l]X_{\mathrm{HS},k}^{*}[l]\}}{\frac{1}{2N}\mathbb{E}\{\Lambda_{h,k,k}^{-1}V_k[l]V_k^{*}[l]\Lambda_{h,k,k}^{-1*}\}} \\ &= \frac{\frac{1}{2N}\mathbb{E}\{X_{\mathrm{HS},k}[l]X_{\mathrm{HS},k}^{*}[l]\}}{\frac{1}{2N}|\Lambda_{k,k}^{-1}|^2\mathbb{E}\{V_k[l]V_k^{*}[l]\}} \\ &= \frac{\mathcal{P}_{\mathrm{X},k,k}}{|\Lambda_{k,k}^{-1}|^2\mathcal{P}_{\mathrm{V},k,k}},\end{aligned} \tag{2.17}$$

where $\mathcal{P}_{\mathrm{V},k,k}$ is the $k^{th}$ diagonal element of $\boldsymbol{\mathcal{P}}_{\mathbf{V}}$. Finally, the nSNR is given by

$$\bar{\gamma}_{\mathrm{V},k} = \frac{1}{|\Lambda_{h,k,k}^{-1}|^2\mathcal{P}_{\mathrm{V},k,k}}. \tag{2.18}$$

Overall, the mathematical deductions presented in this section revisits how the formulation in [50, 51] is applied to deal with a few problems related to the use of the HS-OFDM.

Moreover, these deductions can also be applied to OCDM, SCCP, and OSDM schemes under the presence of the same problems. In this sense, the following research questions are investigated in this thesis:

- Is it possible to extend all these formulation to quantify the same problems in other data communication schemes, such as OCDM, SCCP, and OSDM?
- Is there a framework that is capable of deriving HS-OFDM, OCDM, SCCP, and OSDM from one formulation and allowing their easy exchange when the PLC systems faces distinct environments for performing data communication?

To answer these interesting questions, in Chapter 3, a framework is proposed to model the CP length violation and STO in which the frequency domain equalizer is considered in the formulation. And then, the framework is used to mathematically derive data communication schemes such as the OCDM, SCCP, and OSDM.

# 3 THE PROPOSED FRAMEWORK

Currently, there is a call for having flexible PHY layers that rely on software-defined concepts. A software-defined implementation means that the techniques in the PHY layer can be adapted to ensure that the PHY layer maximizes the use of channel resources for a given set of constraints. Regarding the data communication scheme, we point out that their parameters and type change in a software-defined implementation. Paying attention to the change of the data communication scheme, it is necessary to come up with a few schemes that cover distinct scenarios and constraints and, at the same time, share the same implementation core because it results in less computational efforts, and, as a consequence, less hardware resource, resulting in less energy consumption.

In this regard, this chapter introduces a framework that relies on the fast Fourier transform (FFT) as the core tool for implementing the HS-OFDM, OCDM, SCCP, and OSDM. Consequently, this framework can be used for supporting the implementation of a flexible PHY layer, in which one can change its data communication scheme for dealing with distinct scenarios. Also, it shows that all expressions in Section 2.2 can be straightforwardly extended to address the interference caused by the CP violation and STO in the OCDM, SCCP, and OSDM. Furthermore, it derives closed-form expressions for the estimated signal, SINR, SNR, and nSNR for OCDM, SCCP, and OSDM, and highlights some important conclusions about the usability of each of them under certain circumstances. All mathematical derivations refer to the baseband data communication since the focus is on PLC systems; however, these derivations can be extended to cover the passband data communication.

This chapter is organized as follows: Section 3.1 demonstrates the proposed framework's mathematical deductions; Section 3.2 characterizes the OCDM scheme; Section 3.3 mathematically derives the SCCP scheme, Section 3.4 presents the deductions for the OSDM scheme, and, at last, Section 3.5 displays some general comments.

## 3.1 THE MATHEMATICAL FORMULATION

Considering the interference caused by the CP length violation and STO, the formalization of the proposed framework for encompassing the HS-OFDM, OCDM, SCCP, and OSDM into a unified formulation, that can be useful for changing the data communication scheme in PLC systems facing changing scenarios, relies on the following theorem:

***Theorem*** 1*: If the data communication scheme operates over an $L_h$-length and time-invariant channel impulse response, the additive noise is a random process, the transmitter and receiver matrices are given by $\overline{\mathbf{T}} = \mathbf{\Psi}_t\mathbf{F}^\dagger\mathbf{Q}^\dagger\mathbf{F}$ and $\overline{\mathbf{R}} = \mathbf{F}^\dagger\mathbf{Q}\mathbf{E}\mathbf{F}\mathbf{\Psi}_r$, respectively, which may not ensure that the channel convolution matrix is circulant, and $\mathbf{Q}^\dagger\mathbf{Q} = \mathbf{I}_{2N}$, then the formulation in* (3.6) *can be used to quantify the distortion introduced by the cyclic prefix length violation and symbol time offset.*

*Proof:* Assume that $\overline{\mathbf{T}} = \mathbf{T}\overline{\mathbf{P}}$, $\overline{\mathbf{R}} = \overline{\mathbf{P}}^{\dagger}\mathbf{E}\mathbf{R}$, where $\overline{\mathbf{P}} = \mathbf{Q}^{\dagger}\mathbf{F}$, $\overline{\mathbf{P}}^{\dagger}\overline{\mathbf{P}} = \mathbf{I}_{2N}$, $\mathbf{T} = \mathbf{\Psi}_t\mathbf{F}^{\dagger}$, $\mathbf{R} = \mathbf{F}\mathbf{\Psi}_r$, $\mathbf{\Psi}_t$ is given by (2.5), $\mathbf{\Psi}_r$ is given by (2.7), and the channel equalization is performed in the discrete-frequency domain. Also, let the block diagrams for the framework's transmitter and receiver be shown in Figure 3. Consequently, the $l^{\text{th}}$ $N$-block zero mean WSS random symbol vector, $\overline{\mathbf{x}}[l]$, is properly mapped into a $2N$-block symbol, $\overline{\mathbf{x}}_{\zeta}[l]$, to enable the baseband data communication. Then, the mapped symbol is processed thought the transmitter in the proposed framework by applying the transmitter matrix, which is given by

$$\begin{aligned}\overline{\mathbf{T}} &= \mathbf{\Psi}_t\mathbf{F}\mathbf{Q}^{\dagger}\mathbf{F}^{\dagger} \\ &= \mathbf{T}\overline{\mathbf{P}},\end{aligned} \tag{3.1}$$

where $\mathbf{Q} \in \mathbb{C}^{2N\times 2N}$ is matrix that fulfills a specific constraint (i.e., $\mathbf{Q}^{\dagger}\mathbf{Q} = \mathbf{I}_{2N}$), $\mathbf{\Psi}_t$ is the CP insertion matrix. $\overline{\mathbf{P}} = \mathbf{Q}^{\dagger}\mathbf{F}$ is the generic precoding matrix, which brings $\overline{\mathbf{x}}_{\zeta}[l]$ to the discrete-frequency domain. Therefore, the $\tilde{N}$-block symbol sent by the transmitter in the proposed framework is given by

$$\begin{aligned}\mathbf{x}[l] &= \overline{\mathbf{T}}\overline{\mathbf{x}}_{\zeta}[l] \\ &= \mathbf{T}\overline{\mathbf{P}}\overline{\mathbf{x}}_{\zeta}[l] \\ &= \mathbf{\Psi}_t\mathbf{F}^{\dagger}\mathbf{\Gamma}_{\text{HS}}^{\dagger}\mathbf{F}\overline{\mathbf{x}}_{\zeta}[l].\end{aligned} \tag{3.2}$$

As for the framework reception, the matrix representation of the receiver is given by

$$\begin{aligned}\overline{\mathbf{R}} &= \mathbf{F}^{\dagger}\mathbf{Q}\mathbf{E}\mathbf{F}\mathbf{\Psi}_r \\ &= \overline{\mathbf{P}}^{\dagger}\mathbf{E}\mathbf{R},\end{aligned} \tag{3.3}$$

where $\overline{\mathbf{P}}^{\dagger} = \mathbf{F}^{\dagger}\mathbf{Q}$ ensures that $\overline{\mathbf{P}}^{\dagger}\overline{\mathbf{P}} = \mathbf{I}_{2N}$ and $\mathbf{E}$[1] is the mathematical representation of the discrete-frequency domain equalizer, and $\mathbf{R} = \mathbf{F}\mathbf{\Psi}_r$. Now, as the proposed framework dictates, let the vector representation of the received $l^{\text{th}}$ $2N$-block symbol, at the input of the receiver in the proposed framework, be given by

$$\begin{aligned}\mathbf{y}[l] &\triangleq \sum_{i=-1}^{I}\mathbf{H}[-i]\overline{\mathbf{T}}\overline{\mathbf{x}}_{\zeta}[l-i] + \mathbf{v}[l] \\ &= \mathbf{H}[0]\overline{\mathbf{T}}\overline{\mathbf{x}}_{\zeta}[0] + \sum_{\substack{i=-1 \\ i\neq 0}}^{I}\mathbf{H}[-i]\overline{\mathbf{T}}\overline{\mathbf{x}}_{\zeta}[l-i] + \mathbf{v}[l]\end{aligned} \tag{3.4}$$

where $\overline{\mathbf{x}}_{\zeta}[l-i]$ is the $(l-i)^{\text{th}}$ mapped $2N$-block modulated signal. The vector recovery is made through the receiver in the proposed framework, which includes the equalization process. The

[1] The equalizer is included in $\overline{\mathbf{R}}$ because the equalization in the discrete-frequency domain is simpler than the other domains contemplated in this thesis. If the channel frequency response is flat and zero gain, then $\mathbf{E} = \mathbf{I}_{2N}$.

Figure 3 – Block diagrams of the generic framework's transmitter and receiver.

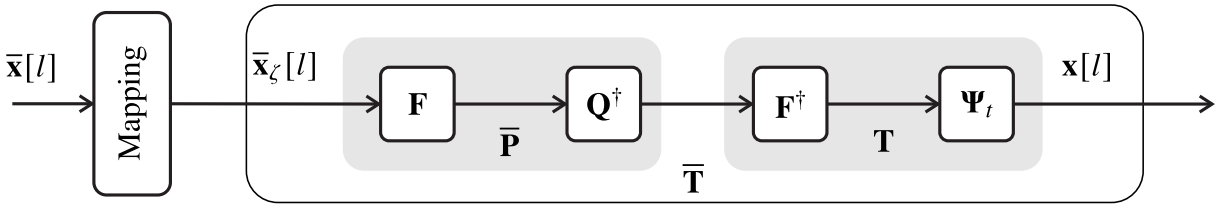


(a) Transmitter

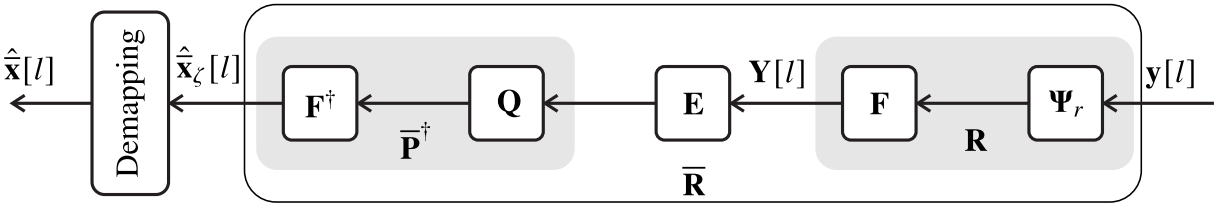


(b) Receiver

vector representation of the received $l^{\text{th}}$ $2N$-block symbol in the discrete-frequency domain is given by

$$\begin{aligned}\mathbf{Y}[l] &= \mathbf{F}\mathbf{\Psi}_r\mathbf{y}[l] \\ &= \mathbf{R}\mathbf{y}[l] \\ &= \mathbf{R}\mathbf{H}[0]\mathbf{T}\overline{\mathbf{P}}\overline{\mathbf{x}}_\zeta[l] + \sum_{\substack{i=-1 \\ i\neq 0}}^{I} \mathbf{R}\mathbf{H}[-i]\mathbf{T}\overline{\mathbf{P}}\overline{\mathbf{x}}_\zeta[l-i] + \mathbf{R}\mathbf{v}[l] \\ &= \mathbf{A}[0]\overline{\mathbf{P}}\dot{\mathbf{x}}_\zeta[l] + \sum_{\substack{i=-1 \\ i\neq 0}}^{I} \mathbf{A}[i]\overline{\mathbf{P}}\dot{\mathbf{x}}_\zeta[l-i] + \mathbf{V}[l]\end{aligned} \tag{3.5}$$

with $\mathbf{V}[l] = \mathbf{R}\mathbf{v}[l] \in \mathbb{C}^{2N\times 1}$ being the vector representation of the noise in the discrete-frequency domain.

A comparison between (2.8), from Section 2.2, and (3.5) shows that both of them behave in a similar manner, with the precoding matrix $\overline{\mathbf{P}}$ being the major difference between the two of them. The equalization process is also conducted in the discrete-frequency domain and it is given by (2.9).

Since the vector is now in the discrete-frequency domain, the equalization is performed in the mentioned domain by using $\mathbf{E}$. Moreover, it is applied $\overline{\mathbf{P}}^\dagger$ so an estimated vector can be retrieved from (3.5). Note that $\overline{\mathbf{P}}^\dagger$ brings back the vector from the discrete-frequency domain. Therefore,

the $l^{\text{th}}$ estimated $2N$-block symbol, $\hat{\overline{\mathbf{x}}}_{\zeta}[l]$, is given by

$$\begin{aligned}
\hat{\overline{\mathbf{x}}}_{\zeta}[l] &\triangleq \overline{\mathbf{P}}^{\dagger}\mathbf{E}\mathbf{Y}[l] \\
&= \sum_{\substack{i=-1 \\ i\neq 0}}^{I} \overline{\mathbf{R}}\mathbf{H}[-i]\overline{\mathbf{T}}\overline{\mathbf{x}}_{\zeta}[l-i] + \overline{\mathbf{R}}\mathbf{v}[l] \\
&= \overline{\mathbf{P}}^{\dagger}\mathbf{E}\mathbf{A}[0]\overline{\mathbf{P}}\overline{\mathbf{x}}_{\zeta}[l] + \sum_{\substack{i=-1 \\ i\neq 0}}^{I} \overline{\mathbf{P}}^{\dagger}\mathbf{E}\mathbf{A}[i]\overline{\mathbf{P}}\overline{\mathbf{x}}_{\zeta}[l-i] + \overline{\mathbf{P}}^{\dagger}\mathbf{E}\mathbf{V}[l] \\
&= \overline{\mathbf{A}}[0]\overline{\mathbf{x}}_{\zeta}[l] + \sum_{\substack{i=-1 \\ i\neq 0}}^{I} \overline{\mathbf{A}}[i]\overline{\mathbf{x}}_{\zeta}[l-i] + \overline{\mathbf{P}}^{\dagger}\mathbf{E}\mathbf{V}[l] \\
&= \mathcal{D}\{\overline{\mathbf{A}}[0]\}\overline{\mathbf{x}}_{\zeta}[l] + \overline{\mathcal{D}}\{\overline{\mathbf{A}}[0]\}\overline{\mathbf{x}}_{\zeta}[l] + \sum_{\substack{i=-1 \\ i\neq 0}}^{I} \overline{\mathbf{A}}[i]\overline{\mathbf{x}}_{\zeta}[l-i] + \overline{\mathbf{G}}\mathbf{V}[l],
\end{aligned} \tag{3.6}$$

where $\overline{\mathbf{A}}[i] = \overline{\mathbf{P}}^{\dagger}\mathbf{E}\mathbf{A}[i]\overline{\mathbf{P}}$ and $\overline{\mathbf{G}} = \overline{\mathbf{P}}^{\dagger}\mathbf{E}$. The above expression shows that the desired vector, $\mathcal{D}\{\overline{\mathbf{A}}[0]\}\overline{\mathbf{x}}_{\zeta}[l]$, is being disturbed by both interference, represented by $\overline{\mathcal{D}}\{\overline{\mathbf{A}}[0]\}\overline{\mathbf{x}}_{\zeta}[l]$ and $\sum_{\substack{i=-1 \\ i\neq 0}}^{I} \overline{\mathbf{A}}[i]\overline{\mathbf{x}}_{\zeta}[l-i]$, and the additive noise, $\overline{\mathbf{G}}\mathbf{V}[l]$. Finally, the demapping process is the last step for the receiver in the proposed framework, turning the estimated mapped $2N$-block symbol in the estimated $N$-block symbol $\hat{\overline{\mathbf{x}}}[l]$. □

Furthermore, the interference disturbing the data communication system can be classified in two types. The first is the ISI, which is the interference caused by the $(l-i)^{\text{th}}$ block signal for $i = -1, 1, \ldots, I$, at the $l^{\text{th}}$ desired block signal and the diagonal elements of $\overline{\mathbf{A}}[i]$, $i = -1, 1, \ldots, I$, contributes with this kind of interference. The second type depends on the adopted data communication scheme once the $\mathbf{Q}$ matrix is defined and is addressed in Sections 3.2, 3.3, and 3.4. Moreover, those interference can be removed from the data communication system if the following constraints are taken into account:

- Values of $L_{cp} \geq L_h$ results in $\overline{\mathbf{A}}[i] = \mathbf{0}_{2N}$ for $i = 1, \ldots, I$.
- The value of $\Delta = 0$ results in $\overline{\mathbf{A}}[-1] = \mathbf{0}_{2N}$ .
- If both of the aforementioned constrains are adopted, then the data communication is free of interference, meaning that

$$\overline{\mathbf{A}}[i] = \begin{cases} \mathbf{I}_{2N} & \text{for } i = 0 \\ \mathbf{0}_{2N} & \text{for } i = -1, 1, \ldots, I. \end{cases} \tag{3.7}$$

In this sense, with the absence of interference, the only form of disturbance left in (3.6) is the additive noise. Therefore, the estimated $2N$-block signal expression reduces to

$$\hat{\overline{\mathbf{x}}}_{\zeta}[l] = \overline{\mathbf{x}}_{\zeta}[l] + \overline{\mathbf{G}}\mathbf{V}[l]. \tag{3.8}$$

The SINR analysis for the generic formulation also follows the one made with the HS-OFDM scheme in Section 2.2. Consequently, it is possible to name the components in the right side of (3.6) as follows:

- $\mathcal{D}\{\overline{\mathbf{A}}[0]\}\overline{\mathbf{x}}_\zeta[l]$ being the desired signal.
- $\overline{\mathcal{D}}\{\overline{\mathbf{A}}[0]\}\overline{\mathbf{x}}_\zeta[l] + \sum_{\substack{i=-1\\ i\neq 0}}^{I} \overline{\mathbf{A}}[i]\overline{\mathbf{x}}_\zeta[l-i]$ being the interference.
- $\overline{\mathbf{G}}\mathbf{V}[l]$ being the additive noise.

In this sense, the desired signal power matrix is given by

$$\begin{aligned}\overline{\mathcal{P}}_{\mathbf{S}} &= \frac{1}{2N}\mathcal{D}\{\overline{\mathbf{A}}[0]\}\mathbb{E}\{\overline{\mathbf{x}}_\zeta[l]\overline{\mathbf{x}}_\zeta^\dagger[l]\}\mathcal{D}\{\overline{\mathbf{A}}[0]\}^\dagger \\ &= \mathcal{D}\{\overline{\mathbf{A}}[0]\}\mathcal{P}_{\mathbf{x}}\mathcal{D}\{\overline{\mathbf{A}}[0]\}^\dagger\end{aligned} \tag{3.9}$$

where $\mathcal{P}_{\mathbf{x}} = \mathbb{E}\{\overline{\mathbf{x}}_\zeta[l]\overline{\mathbf{x}}_\zeta^\dagger[l]\}/2N$. While the interference-plus-noise power matrix is defined by

$$\begin{aligned}\overline{\mathcal{P}}_{\mathbf{IV}} \triangleq\ & \frac{1}{2N}\overline{\mathcal{D}}\{\overline{\mathbf{A}}[0]\}\mathbb{E}\{\overline{\mathbf{x}}_\zeta[l]\overline{\mathbf{x}}_\zeta^\dagger[l]\}\overline{\mathcal{D}}\{\overline{\mathbf{A}}[0]\}^\dagger + \\ & \frac{1}{2N}\sum_{\substack{i=-1\\ i\neq 0}}^{I} \overline{\mathbf{A}}[i]\mathbb{E}\{\overline{\mathbf{x}}_\zeta[l-i]\overline{\mathbf{x}}_\zeta^\dagger[l-i]\}\overline{\mathbf{A}}^\dagger[i] + \frac{1}{2N}\overline{\mathbf{G}}\mathbb{E}\{\mathbf{V}[l]\mathbf{V}^\dagger[l]\}\overline{\mathbf{G}}^\dagger \\ =\ & \overline{\mathcal{D}}\{\overline{\mathbf{A}}[0]\}\overline{\mathcal{P}}_{\mathbf{x}}\overline{\mathcal{D}}\{\overline{\mathbf{A}}[0]\}^\dagger + \sum_{\substack{i=-1\\ i\neq 0}}^{I} \overline{\mathbf{A}}[i]\overline{\mathcal{P}}_{\mathbf{x}}\overline{\mathbf{A}}^\dagger[i] + \overline{\mathbf{G}}\mathcal{P}_{\mathbf{V}}\overline{\mathbf{G}}^\dagger.\end{aligned} \tag{3.10}$$

At last, the SINR for the $k^{\text{th}}$ symbol of the $2N$-block symbols is equal to

$$\overline{\gamma}_{\text{IV},k} = \frac{\overline{\mathcal{P}}_{\text{S},k,k}}{\overline{\mathcal{P}}_{\text{IV},k,k}}, \tag{3.11}$$

where $\overline{\mathcal{P}}_{\text{S},k,k}$ and $\overline{\mathcal{P}}_{\text{IV},k,k}$ are the $k^{\text{th}}$ diagonal element of $\overline{\mathcal{P}}_{\mathbf{S}}$ and $\overline{\mathcal{P}}_{\mathbf{IV}}$, respectively.

Figure 4 shows how the theorem (i.e., the proposed framework) is applied to obtain the mathematical formulations for the HS-OFDM, OCDM, SCCP, and OSDM schemes. Note that the proposed framework allows the possibility to work with four distinct data communication schemes that can be dynamically switched to deal with specific characteristics of a data communication channel, which in this thesis is the PLC channel.

The Subsections 3.2, 3.3, and 3.4 detail the mathematical derivations from the proposed framework to address OCDM, SCCP, and OSDM schemes, respectively, while Section 2.2 can be reinterpreted as a formulation derived from the proposed framework with respect to the HS-OFDM. Moreover, Subsections 3.2, 3.3, and 3.4 pay attention to differences among the above-mentioned data communication schemes and the circumstances they should be applied.

Figure 4 – Illustration of the proposed framework and the derived schemes.

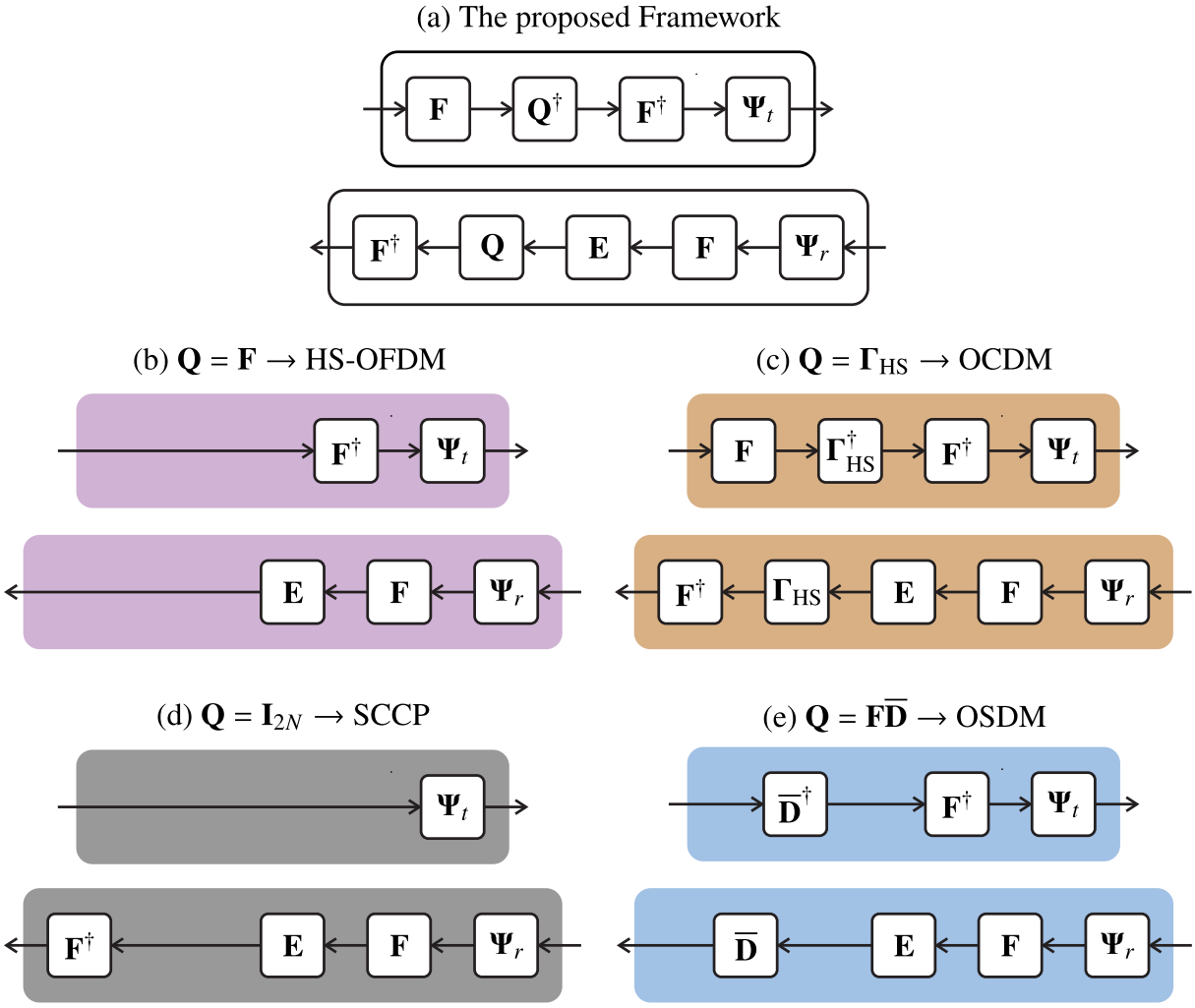


## 3.2 THE OCDM SCHEME

The OCDM uses the DFnT, see Appendix A, to assign a point in a constellation to an orthogonal chirp, with each chirp occupying a changing frequency with time within the time interval of one OCDM symbol, as illustrated in Figure 5(b). Let the block diagrams for the OCDM transmitter and receiver be shown in Figure 4(c). With the adoption of the type-IV mapping described in [49], the deduction of the OCDM for baseband data communication is as follows: The first step is the extension of the $N$-block modulated signal in the discrete-Fresnel domain, $\overline{\mathbf{x}} \in \mathbb{C}^{N\times 1}$, into the $2N$-block symbol, $\overline{\mathbf{x}}_\zeta \in \mathbb{R}^{2N\times 1}$, using the following expression:

$$\overline{x}_{\zeta,k}[l] = \begin{cases} \sqrt{2}\Re\{\overline{x}_k[l]\}, & k = 0,\ldots,N-1 \\ \sqrt{2}\Im\{\overline{x}_{k-N}[l]\}, & k = N,\ldots,2N-1 \end{cases}. \tag{3.12}$$

Then, it is considered the matrix $\mathbf{Q} = \mathbf{\Gamma}_{\text{HS}}$, making $\overline{\mathbf{P}} = \mathbf{\Gamma}_{\text{HS}}\mathbf{F}$, with $\mathbf{\Gamma}_{\text{HS}}$ being the artificial Hermitian symmetric phase diagonal matrix [49] with elements given by

$$\Gamma_{\text{HS},k,k} = \begin{cases} e^{-j\frac{\pi}{2N}k^2}, & \text{for } 0 \leq k \leq N-1 \\ e^{j\frac{\pi}{2N}k^2}, & \text{for } N-1 < k \leq 2N-1 \end{cases}. \tag{3.13}$$

This condition transforms the proposed framework into the OCDM scheme, since the DFnT is equal to $\mathbf{\Phi}_{\text{HS}} = \mathbf{F}^{\dagger}\mathbf{\Gamma}_{\text{HS}}\mathbf{F}$. Additional and necessary information about the DFnT can be found in Appendix A. Therefore, the OCDM transmitter is given by

$$\begin{aligned} \overline{\mathbf{T}} &= \mathbf{\Psi}_t\mathbf{\Phi}_{\text{HS}}^{\dagger} \\ &= \mathbf{\Psi}_t\mathbf{F}^{\dagger}\mathbf{\Gamma}_{\text{HS}}^{\dagger}\mathbf{F} \\ &= \mathbf{T}\overline{\mathbf{P}}. \end{aligned} \tag{3.14}$$

As for the reception, the matrix representation of the receiver is given by

$$\begin{aligned} \overline{\mathbf{R}} &= \mathbf{F}^{\dagger}\mathbf{\Gamma}_{\text{HS}}\mathbf{E}\mathbf{F}\mathbf{\Psi}_r, \\ &= \overline{\mathbf{P}}^{\dagger}\mathbf{E}\mathbf{R}, \end{aligned} \tag{3.15}$$

where $\overline{\mathbf{P}}^{\dagger} = \mathbf{F}^{\dagger}\mathbf{\Gamma}_{\text{HS}}$. Now, the two final necessary terms to characterize the OCDM estimated signal and SINR left are the $\overline{\mathbf{A}}[i]$ and $\overline{\mathbf{G}}$. The first one is given by

$$\begin{aligned} \overline{\mathbf{A}}[i] &= \overline{\mathbf{R}}\mathbf{H}[i]\overline{\mathbf{T}} \\ &= \mathbf{F}^{\dagger}\mathbf{\Gamma}_{\text{HS}}\mathbf{E}\mathbf{F}\mathbf{\Psi}_r\mathbf{H}[i]\mathbf{\Psi}_t\mathbf{F}^{\dagger}\mathbf{\Gamma}_{\text{HS}}^{\dagger}\mathbf{F} \\ &= \mathbf{F}^{\dagger}\mathbf{\Gamma}_{\text{HS}}\mathbf{E}\mathbf{A}[i]\mathbf{\Gamma}_{\text{HS}}^{\dagger}\mathbf{F} \\ &= \overline{\mathbf{P}}^{\dagger}\mathbf{E}\mathbf{A}[i]\overline{\mathbf{P}}. \end{aligned} \tag{3.16}$$

and the second one is equal to

$$\begin{aligned} \overline{\mathbf{G}} &= \overline{\mathbf{P}}^{\dagger}\mathbf{E} \\ &= \mathbf{F}^{\dagger}\mathbf{\Gamma}_{\text{HS}}\mathbf{E}. \end{aligned} \tag{3.17}$$

The expressions (3.16) and (3.17) are used to obtain the proper expression of estimated $2N$-block symbol, given by (3.6), when the OCDM scheme is being considered.

The last step required to complete the data communication system is to apply the demapping process, which generates $\hat{\mathbf{x}}[l]$, whose $k^{\text{th}}$ subchirp are given by

$$\hat{\tilde{x}}_k[l] = \frac{1}{\sqrt{2}}\hat{\tilde{x}}_{\zeta,k}[l] + \frac{1}{\sqrt{2}}j\hat{\tilde{x}}_{\zeta,k+N}[l], \tag{3.18}$$

for $k = 0, \ldots, N-1$. Furthermore, the second type of interference disturbing the estimated signal can be categorize as inter-chirp interference (ICpI) which is the caused by subchirps from the $(l-i)^{\text{th}}$ block signal, $i = -1, 0, 1, \ldots, I$. The non-diagonal elements of $\overline{\mathbf{A}}[i]$, $i = -1, 0, 1, \ldots, I$, contributes with this kind interference. The SINR is given by (3.11).

If the data communication is free from interference, the sample associated with the $k^{\text{th}}$ subchirp of (3.8) is equal to

$$\hat{\overline{x}}_{\zeta,k}[l] = \overline{x}_{\zeta,k}[l] + \frac{1}{\sqrt{2N}} \sum_{i=0}^{2N-1} e^{j\frac{2\pi}{2N}ki} e^{-j\frac{\pi}{2N}i^2} \Lambda_{h,i,i}^{-1} V_i[l] \tag{3.19}$$

So, the SNR for the $k^{\text{th}}$ subchirp is equal to

$$\begin{aligned}\overline{\gamma}_{\text{V},k} &= \frac{\frac{1}{2N}\mathbb{E}\{\overline{x}_{\zeta,k}[l]\overline{x}^*_{\zeta,k}[l]\}}{\frac{1}{2N}\mathbb{E}\left\{\left(\frac{1}{\sqrt{2N}}\sum_{i=0}^{2N-1} e^{j\frac{2\pi}{2N}ki} e^{-j\frac{\pi}{2N}i^2}\Lambda_{h,i,i}^{-1} V_i[l]\right)\left(\frac{1}{\sqrt{2N}}\sum_{i=0}^{2N-1} e^{-j\frac{2\pi}{2N}ki} e^{j\frac{\pi}{2N}i^2}\Lambda_{h,i,i}^{*-1} V_i^*[l]\right)\right\}} \\ &= \frac{\overline{\mathcal{P}}_{\text{x},k,k}}{\frac{1}{2N}\sum_{i=0}^{2N-1}\sum_{i'=0}^{2N-1} e^{j\frac{2\pi}{2N}ki} e^{-j\frac{\pi}{2N}i^2} e^{-j\frac{2\pi}{2N}ki'} e^{j\frac{\pi}{2N}i'^2}\Lambda_{h,i,i}^{-1}\Lambda_{h,i',i'}^{-1*}\frac{1}{2N}\mathbb{E}\{V_i[l]V_{i'}^*[l]\}},\end{aligned} \tag{3.20}$$

and since $V_i[l]$ is a zero-mean WSS Gaussian random process, $\mathbb{E}\{V_i[l]\} = 0$ and $\mathbb{E}\{V_i[l]V_{i'}^*[l]\} = \mathbb{E}\{V_i[l]\}\mathbb{E}\{V_{i'}^*[l]\}$, $\forall i \neq i'$. Therefore, the SNR results in

$$\begin{aligned}\overline{\gamma}_{\text{V},k} &= \frac{\overline{\mathcal{P}}_{\text{x},k,k}}{\frac{1}{2N}\sum_{i=0}^{2N-1}|e^{j\frac{2\pi}{2N}ki}|^2|e^{-j\frac{\pi}{2N}i^2}|^2|\Lambda_{h,i,i}^{-1}|^2\frac{1}{2N}\mathbb{E}\{V_i[l]V_i^*[l]\}} \\ &\triangleq \frac{\overline{\mathcal{P}}_{\text{x},k,k}}{\frac{1}{2N}\sum_{i=0}^{2N-1}|\Lambda_{h,i,i}^{-1}|^2\mathcal{P}_{\text{V},i,i}}.\end{aligned} \tag{3.21}$$

In contrast to [48], which considers only white noise for the mathematical development, (3.21) displays a general SNR expression for the OCDM when the additive noise is, at least, a WSS random process. Moreover, the SNR of the SCCP found in [26, Section III-C] is equal to the SNR expression in (3.21), if the additive noise is modeled as a zero mean and white random process. Next, the nSNR for all subchirps is the same value, which is given by

$$\begin{aligned}\bar{\overline{\gamma}}_{\text{V},k} &= \frac{1}{\frac{1}{2N}\sum_{i=0}^{2N-1}|\Lambda_{h,i,i}^{-1}|^2\mathcal{P}_{\text{V},i,i}} \\ &\triangleq \left(\frac{1}{2N}\sum_{i=0}^{2N-1}\bar{\gamma}_{\text{V},i}^{-1}\right)^{-1}.\end{aligned} \tag{3.22}$$

In other words, the nSNR for the OCDM always has the same value, despite its subchirp, and is given by the harmonic mean of the elements of $\bar{\gamma}_V = [\bar{\gamma}_{V,0}, \ldots, \bar{\gamma}_{V,2N-1}]^T$. It is important to emphasize the existing similarity between (3.22) and the nSNR of OSDM found in [28], which is highlighted in Section 3.4. Note that (3.22) covers all frequency bandwidth, since it performs the harmonic mean throughout the subbands, while the one cited in [28] performs a sequence of harmonic means, with each one considering only a given piece of the frequency bandwidth.

Due to the prominence and relevance of the HS-OFDM in the modern data communication systems, a few comments related to a comparison between the OCDM and HS-OFDM are as follows:

- (3.22) and (2.18) are different from each other. The former emphasizes that one subchirp linearly occupies all subbands within the $2N$-block symbol period, which is the reason for having a harmonic mean, while the latter assumes that one subcarrier occupies a given frequency subband within the $2N$-block symbol period.
- (3.22) states that all subchirps transmit the same amount of bits meaning that UA attains the same result of OA. And, more impressive, is the fact that the knowledge of the nSNR of only one subchirp is enough to allocate bits in all subchirps, which remarkably simplify the resource allocation process. On the other hand, (2.18) takes advantage of bit loading techniques, mainly OA, to maximize data rate; however, it demands the knowledge of the nSNR of all subchannels.
- (3.22) shows that the OCDM performs an elegant combination of the frequency selective of the channel and the colored additive noise to result in the same nSNR in all subchirps, which is the opposite from what is observed in (2.18).
- If the channel frequency response is flat and corrupted by the AWGN, then (3.22) and (2.18) result in the same nSNR values.

Overall, a comparison between OCDM and HS-OFDM allows the following statements to be made:

- The OCDM scheme can successfully replace the HS-OFDM one due to a couple of interesting advantages. Firstly, the OCDM is more robust (i.e., less sensitive to CP length violation) and offers better bit error probability when the CSI is not available at the transmitter side and adaptive modulation applies, as numerically shown in Chapter 4. Secondly, the availability of the CSI at the transmitter side allows the transition of OCDM to HS-OFDM, to take advantage of a bit loading technique for maximizing data rates.
- The whole deduction presented in Section 2.2 can be extended to mathematically quantify the impact of the CP length violation and the STO. The former quantification is very interesting because, for the first time, closed-form expressions are used to address it in the OCDM. The latter quantification allowed the extension of the OCDM analysis beyond what has been found in the literature.

Moreover, it is possible to interpret the OCDM scheme as a precoded version of the HS-OFDM one, since $\overline{\mathbf{T}} = \mathbf{T}\boldsymbol{\Gamma}_{\mathrm{HS}}^{\dagger}\mathbf{F} = \mathbf{T}\overline{\mathbf{P}}$ and $\overline{\mathbf{R}} = \mathbf{F}^{\dagger}\boldsymbol{\Gamma}_{\mathrm{HS}}\mathbf{E}\mathbf{R} = \overline{\mathbf{P}}^{\dagger}\mathbf{E}\mathbf{R}$, where $\overline{\mathbf{P}} = \boldsymbol{\Gamma}_{\mathrm{HS}}^{\dagger}\mathbf{F}$ is the specific pre-coding matrix for the OCDM.

Finally, the mathematical formulation of the OCDM scheme shows that it is a useful data communication scheme when the CSI is unavailable at the transmitter side [52], or when there is CP length violation [49]. Also, it is attractive under the presence of STO, which is numerically shown in Chapter 4.

## 3.3 THE SCCP SCHEME

This subsection deduces the closed-form expression for the SCCP scheme. Similar to Subsection 3.2, it derives the estimated signal, SINR, and SNR. It is important to emphasize that the SCCP scheme is a well-known data communication scheme that uses the entire bandwidth for transmitting each symbol [26, 27], which is referred to in this thesis as subsymbol. Based on the proposed Framework, it is necessary to consider $\mathbf{Q} = \mathbf{I}_{2N}$ for attaining the SCCP scheme, as illustrated in Figure 4(d). As the data communication is in the baseband, it is necessary to use mapping and demapping given by (3.12) and (3.18), respectively, if two-dimensions digital modulation are considered (e.g., $M$-QAM). Note that the mapping and demapping are not necessary if one-dimension digital modulation applies (e.g., $M$-pulse amplitude modulation (PAM)). Therefore, the SCCP transmitter is given by

$$\overline{\mathbf{T}} = \mathbf{\Psi}_t, \tag{3.23}$$

and the receiver is given by

$$\overline{\mathbf{R}} = \mathbf{F}^{\dagger}\mathbf{E}\mathbf{F}\mathbf{\Psi}_r. \tag{3.24}$$

The equations 3.23 and 3.24 are illustrated in Figure 4(d). Next, one only needs to obtain the following terms to be able to characterize the SCCP scheme:

$$\begin{aligned}\overline{\mathbf{A}}[i] &= \overline{\mathbf{R}}\mathbf{H}[-i]\overline{\mathbf{T}} \\ &= \mathbf{F}^{\dagger}\mathbf{E}\mathbf{F}\mathbf{\Psi}_r\mathbf{H}[-i]\mathbf{\Psi}_t \\ &= \mathbf{F}^{\dagger}\mathbf{E}\mathbf{A}[i]\mathbf{F}\end{aligned} \tag{3.25}$$

and

$$\overline{\mathbf{G}} = \mathbf{F}^{\dagger}\mathbf{E}. \tag{3.26}$$

With (3.25) and (3.26) in hand, one can obtain the estimated $2N$-block symbol for the SCCP scheme, which is given by (3.6), from Theorem 1. The second type of interference disturbing the estimated signal is called inter-slot interference (IStI) which is caused by subsymbols from the $(l-i)^{\text{th}}$ $2N$-block signal, $i = -1, 0, 1, \ldots, I$, with the non-diagonal elements of $\overline{\mathbf{A}}[i]$, $i = -1, 0, 1, \ldots, I$, contributing with this kind interference. Moreover, the SCCP SINR expressionis given by (3.11) and SNR expressions can be easily derived. When there is no interference in the communication (i.e. $L_{cp} \geq L_h$ and $\Delta = 0$), the $k^{\text{th}}$ symbol of the estimated mapped signal is given by

$$\hat{\overline{x}}_{\zeta,k}[l] = \overline{x}_{\zeta,k}[l] + \frac{1}{\sqrt{2N}} \sum_{i=0}^{2N-1} e^{j\frac{2\pi}{2N}ki} \Lambda^{-1}_{h,i,i} V_i[l] \tag{3.27}$$

So, the SNR of the $k^{\text{th}}$ term is equal to

$$\begin{aligned}\overline{\gamma}_{\mathrm{V},k} &= \frac{\frac{1}{2N}\mathbb{E}\{\overline{x}_{\zeta,k}[l]\overline{x}^{*}_{\zeta,k}[l]\}}{\frac{1}{2N}\mathbb{E}\left\{\left(\frac{1}{\sqrt{2N}}\sum_{i=0}^{2N-1} e^{j\frac{2\pi}{2N}ki}\Lambda^{-1}_{h,i,i}V_i[l]\right)\left(\frac{1}{\sqrt{2N}}\sum_{i=0}^{2N-1} e^{-j\frac{2\pi}{2N}ki}\Lambda^{*-1}_{h,i,i}V^{*}_i[l]\right)\right\}} \\ &= \frac{\overline{\mathcal{P}}_{\mathrm{x},k,k}}{\frac{1}{2N}\sum_{i=0}^{2N-1}\sum_{i'=0}^{2N-1} e^{j\frac{2\pi}{2N}ki}e^{-j\frac{2\pi}{2N}ki'}\Lambda^{-1}_{h,i,i}\Lambda^{-1*}_{h,i',i'}\frac{1}{2N}\mathbb{E}\{V_i[l]V^{*}_{i'}[l]\}} \\ &= \frac{\overline{\mathcal{P}}_{\mathrm{x},k,k}}{\frac{1}{2N}\sum_{i=0}^{2N-1}|e^{j\frac{2\pi}{2N}ki}|^2\Lambda^{-1}_{h,i,i}|^2\frac{1}{2N}\mathbb{E}\{V_i[l]V^{*}_{i}[l]\}} \\ &= \frac{\overline{\mathcal{P}}_{\mathrm{x},k,k}}{\frac{1}{2N}\sum_{i=0}^{2N-1}|\Lambda^{-1}_{h,i,i}|^2\mathcal{P}_{\mathrm{V},i,i}}.\end{aligned} \tag{3.28}$$

Moreover, the nSNR for all subsymbols is given by

$$\begin{aligned}\bar{\overline{\gamma}}_{\mathbf{V}} &= \frac{1}{\frac{1}{2N}\sum_{i=0}^{2N-1}|\Lambda^{-1}_{h,i,i}|^2\mathcal{P}_{\mathrm{V},i,i}} \\ &= \left(\frac{1}{2N}\sum_{i=0}^{2N-1}\bar{\gamma}^{-1}_{\mathrm{V},i}\right)^{-1}.\end{aligned} \tag{3.29}$$

Last but not least, the comparison between (3.21) with (3.28), and (3.22) with (3.29) shows that the SNR and nSNR of both data communication schemes has the same value. Meaning that both the OCDM and SCCP schemes has the same curves of data rate and bit error probability for a data communication system free of interference. However, the same conclusion can not be stated when comparing the SINR, since each data communication scheme deals with the considered interference in different manners.

## 3.4 THE OSDM SCHEME

The OSDM scheme was proposed in [28]. It is a data communication scheme that utilizes the DOST to divide the time-frequency space into orthogonal tiles bounded by a $\mathcal{B}$-geometry, which is defined in the time frequency domain [29]. The tiles presents different dimensions, as illustrated in Figure 5(d).

The derivation of the SINR and SNR using the proposed framework as the baseline is as follows: first of all, define $\mathbf{Q} = \mathbf{F}\overline{\mathbf{D}}$, with $\mathbf{D} = \overline{\mathbf{D}}\mathbf{F}$ being the DOST and the elements of $\overline{\mathbf{D}}$ are equal to

$$\overline{D}_{k,i} = \begin{cases} \frac{1}{\sqrt{\beta_k}}e^{j2\pi\frac{\tau_k}{\beta_k}i}e^{-j\pi\tau_k} & \nu_k - \lfloor\beta_k/2\rfloor \leq i \leq \nu_k + \lceil\beta_k/2\rceil - 1 \\ 0, & \text{otherwise,}\end{cases} \tag{3.30}$$

where $\lfloor z\rfloor = \max\{n \in \mathbb{Z} | n \leq z\}$. And, the parameters $\nu_k$, $\beta_k$, and $\tau_k$ are elements of the vectors $\boldsymbol{\nu}$, $\boldsymbol{\beta}$, and $\boldsymbol{\tau}$, respectively, and are responsible for the creation of each tile. A more detailed explanation of these parameters can be found in Appendix B.

Further, since the data communication system in this thesis is in the baseband, the Hermitian symmetric mapping and demmaping from (2.3) and (2.12), respectively, can be used in the baseband version of the OSDM.

In Figure 4(e) is illustrated the block-diagram for the OSDM transmitter and receiver. The OSDM transmitter matrix is given by

$$\overline{\mathbf{T}} = \mathbf{\Psi}_t \mathbf{F}^{\dagger} \overline{\mathbf{D}}^{\dagger}, \tag{3.31}$$

and the OSDM receiver matrix is expressed as

$$\overline{\mathbf{R}} = \overline{\mathbf{D}} \mathbf{E} \mathbf{F} \mathbf{\Psi}_t. \tag{3.32}$$

Now, with the possession of the transmitter and receiver matrices, the terms $\overline{\mathbf{A}}[i]$ and $\overline{\mathbf{G}}$ can be obtained. So, the former is given by

$$\begin{aligned} \overline{\mathbf{A}}[i] &= \overline{\mathbf{R}} \mathbf{H}[-i] \overline{\mathbf{T}} \\ &= \overline{\mathbf{D}} \mathbf{E} \mathbf{F} \mathbf{\Psi}_t \mathbf{H}[-i] \mathbf{\Psi}_t \mathbf{F}^{\dagger} \overline{\mathbf{D}}^{\dagger} \\ &= \overline{\mathbf{D}} \mathbf{E} \mathbf{A}[i] \overline{\mathbf{D}}^{\dagger} \end{aligned} \tag{3.33}$$

and the latter is expressed as

$$\overline{\mathbf{G}} = \overline{\mathbf{D}} \mathbf{E}. \tag{3.34}$$

Thus, with the terms of $\overline{\mathbf{A}}[i]$ and $\overline{\mathbf{G}}$ equal to (3.33) and (3.34), respectively, the estimated $2N$-block signal, SINR (3.11) may be derived and they are given by (3.6) and (3.11), respectively.

In regards to the interferences disturbing the data communication system, the second type can be nominated as inter-tile interference (ITI) which is caused by tiles from the $(l-i)^{\text{th}}$ $2N$-block signal, $i = -1, 0, 1, \ldots, I$, with the non-diagonal elements of $\overline{\mathbf{A}}[i]$, $i = -1, 0, 1, \ldots, I$, contributing with this kind interference. Moreover, in the absence of interference, the $k^{\text{th}}$ tile of the estimated $2N$-block signal can be expressed as

$$\hat{\overline{x}}_{\zeta,k}[l] = \overline{x}_{\zeta,k}[l] + \frac{1}{\sqrt{\beta_k}} \sum_{i=\nu_k-\lfloor \beta_k/2 \rfloor}^{\nu_k+\lceil \beta_k/2 \rceil-1} e^{j2\pi \frac{\tau_k}{\beta_k} i} e^{-j\pi\tau_k} \Lambda_{h,i,i}^{-1} V_i[l], \tag{3.35}$$

and, then, the SNR of the $k^{\text{th}}$ tile is given by

$$\begin{aligned} \overline{\gamma}_{\text{V},k} &= \frac{\frac{1}{2N}\mathbb{E}\{\overline{x}_{\zeta,k}[l]\overline{x}^*_{\zeta,k}[l]\}}{\frac{1}{2N}\mathbb{E}\left\{\left(\frac{1}{\sqrt{\beta_k}}\sum_{i=\nu_k-\lfloor\beta_k/2\rfloor}^{\nu_k+\lceil\beta_k/2\rceil-1} e^{j2\pi\frac{\tau_k}{\beta_k}i} e^{-j\pi\tau_k}\Lambda^{-1}_{h,i,i}V_i[l]\right)\left(\frac{1}{\sqrt{\beta_k}}\sum_{i=\nu_k-\lfloor\beta_k/2\rfloor}^{\nu_k+\lceil\beta_k/2\rceil-1} e^{-j2\pi\frac{\tau_k}{\beta_k}i} e^{j\pi\tau_k}\Lambda^{-1*}_{h,i,i}V^*_i[l]\right)\right\}} \\ &= \frac{\overline{\mathcal{P}}_{\text{x},k,k}}{\frac{1}{\beta_k}\sum_{i=\nu_k-\lfloor\beta_k/2\rfloor}^{\nu_k+\lceil\beta_k/2\rceil-1}\sum_{i'=\nu_k-\lfloor\beta_k/2\rfloor}^{\nu_k+\lceil\beta_k/2\rceil-1} e^{j2\pi\frac{\tau_k}{\beta_k}i} e^{-j2\pi\frac{\tau_k}{\beta_k}i'} e^{-j\pi\tau_k} e^{j\pi\tau_k}\Lambda^{-1}_{h,i,i}\Lambda^{-1*}_{h,i',i'}\frac{1}{2N}\mathbb{E}\{V_i[l]V^*_{i'}[l]\}} \\ &= \frac{\overline{\mathcal{P}}_{\text{x},k,k}}{\frac{1}{\beta_k}\sum_{i=\nu_k-\lfloor\beta_k/2\rfloor}^{\nu_k+\lceil\beta_k/2\rceil-1} |e^{j2\pi\frac{\tau_k}{\beta_k}i}|^2|e^{-j\pi\tau_k}|^2|\Lambda^{-1}_{h,i,i}|^2\frac{1}{2N}\mathbb{E}\{V_i[l]V^*_{i'}[l]\}} \\ &= \frac{\overline{\mathcal{P}}_{\text{x},k,k}}{\frac{1}{\beta_k}\sum_{i=\nu_k-\lfloor\beta_k/2\rfloor}^{\nu_k+\lceil\beta_k/2\rceil-1} |\Lambda^{-1}_{h,i,i}|^2\mathcal{P}_{\text{V},i,i}}. \end{aligned} \tag{3.36}$$

Therefore, the nSNR in the $k^{\text{th}}$ tile is given by

$$\begin{aligned}\bar{\bar{\gamma}}_{\mathrm{V},k} &= \frac{1}{\frac{1}{\beta_k}\sum_{i=\nu_k-\lfloor\beta_k/2\rfloor}^{\nu_k+\lceil\beta_k/2\rceil-1}|\Lambda_{h,i,i}^{-1}|^2\mathcal{P}_{\mathrm{V},i,i}} \\ &= \left(\frac{1}{\beta_k}\sum_{i=\nu_k-\lfloor\beta_k/2\rfloor}^{\nu_k+\lceil\beta_k/2\rceil-1}\bar{\gamma}_{\mathrm{V},i}^{-1}\right)^{-1}.\end{aligned} \tag{3.37}$$

At last, the OSDM can be seen as a data communication scheme in between the HS-OFDM and SCCP ones. As a matter of fact, the HS-OFDM and SCCP ones can be considered as a particular case of the OSDM or two oppositve boundaries for the OSDM. For instance:

- If $\beta_k = 1$ for all values of $k$, then $\overline{\mathbf{D}} = \mathbf{I}_{2N}$, $\overline{\mathbf{T}} = \mathbf{T}$, and $\overline{\mathbf{R}} = \mathbf{ER}$. Which means that the OSDM is reduced to the HS-OFDM.
- If $\beta_k = 2N - 1$ for all values of $k$, then $\overline{\mathbf{D}} = \mathbf{F}$, $\overline{\mathbf{T}} = \mathbf{\Psi}_t$, and $\overline{\mathbf{R}} = \mathbf{F}^{\dagger}\mathbf{EF}\mathbf{\Psi}_r$. Which means that the OSDM is reduced to the SCCP.

The fact that the HS-OFDM and SCCP can be derived from the OSDM is very interesting because it emphasizes that its data rate and bit error probability performance will be a midterm between the HS-OFDM and SCCP, and will be closer to either two depending on the adopted $\mathcal{B}$-geometry by the OSDM.

## 3.5 GENERAL COMMENTS

The proposed framework allows one to see the above-mentioned data communication schemes from a singular perspective. Indeed, the nSNR expressions (3.22), (3.29), and (3.37) are very similar to each other, since all of them are harmonic means of the HS-OFDM's nSNR, which is given by (2.18). However, (3.37), which applies to the OSDM scheme, performs the harmonic mean of a consecutive $\beta_k$ subbands, meaning that (3.37) will not have the same value for all tiles, which is different from the OCDM and SCCP. Such characteristics are very important, since it enables the use of the OA technique in OSDM with the aim of improving data rate. Moreover, if the additive noise is modeled as an WSS and uncorrelated random process, and the channel frequency response is flat, then the nSNR of all above mentioned data communication schemes reduces to the same value, which is given by

$$\bar{\bar{\gamma}}_{\mathrm{V},k} = \frac{1}{\mathcal{P}_{\mathrm{V},k,k}}. \tag{3.38}$$

Also, the nSNR of each data communication scheme can be illustrated in the time-frequency dimension that is occupied by one $2N$-block symbol. For instance, Figure 5 illustrates the

existing separation among the occupied band by the subcarriers, subchirps, subsymbols, and tiles when HS-OFDM, OCDM, SCCP, and OSDM are considered, respectively, with $2N = 8$. As the geometric figures occupied by subcarriers, subchirps, and subsymbols can also be seen as distinct tiles, it is clear that the difference among the tile geometries is defined by each of the four data communication schemes. Such difference results in different impacts on the performance of each of them with or without the presence of the CP length violation and STO in the data communication system.

Moreover, some conclusions may be made while comparing these data communication schemes in terms of their nSNR, which are listed in Table 1. For instance, each subcarrier of the HS-OFDM occupies only a single subband and their nSNRs can be different among all subbbands since the CFR and power spectral density (PSD) of the additive noise may not be flat. Meanwhile, each subchirp of the OCDM occupies all the bandwidth, as a consequence, its nSNR is interpreted as the harmonic mean of the nSNR of all subbands that are obtained by using the HS-OFDM. The same can be stated for the SCCP. Regarding the OSDM scheme, since each tile occupies a group of subbands, the nSNR in each tile is the harmonic mean of the nSNR of the HS-OFDM within the group of subbands covered by the tile.

Figure 5 – Tile geometries for the four data communication schemes.

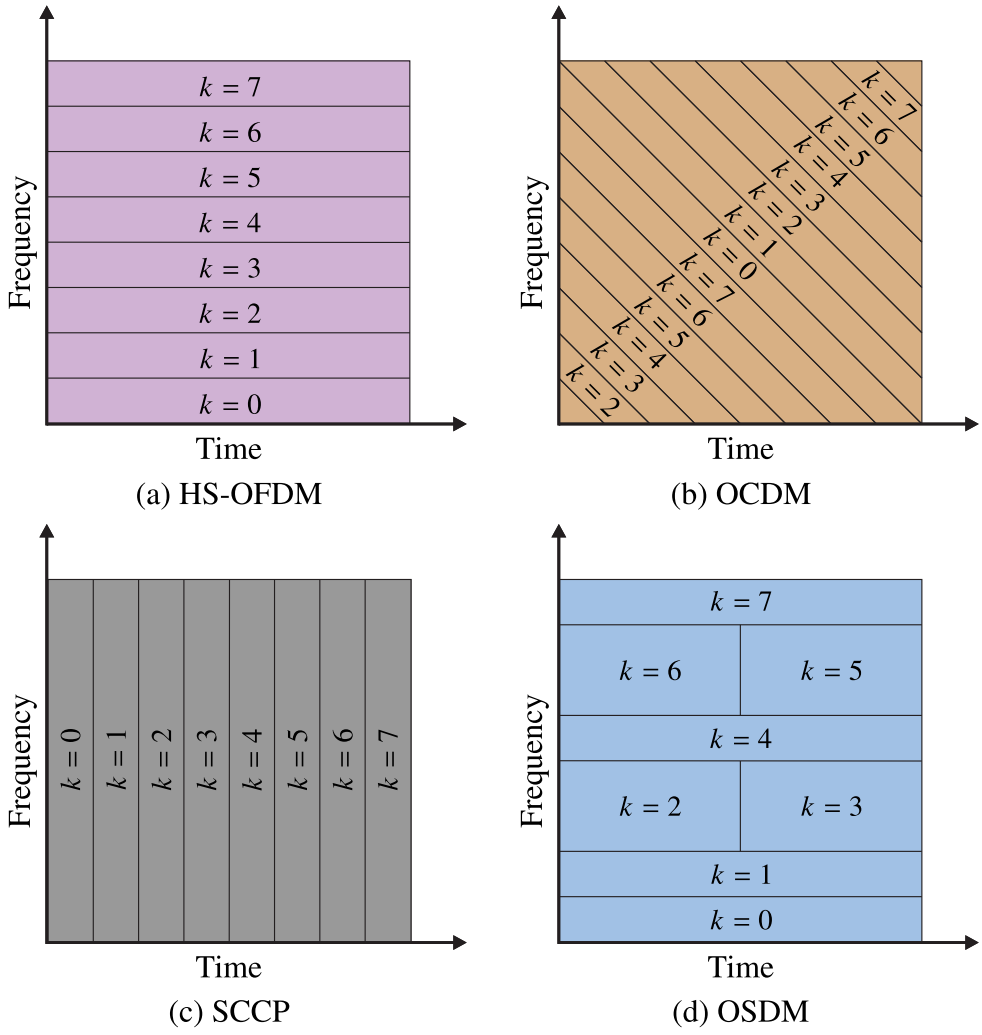

Table 1 − Summary of the nSNR.

| **Data Communication Scheme** | **nSNR** |
|---|---|
| HS-OFDM | $\bar{\gamma}_{\mathrm{V},k} = \frac{1}{\lvert\Lambda^{-1}_{h,k,k}\rvert^2 \mathcal{P}_{\mathrm{V},k,k}}$ for the $k^{\mathrm{th}}$ subcarrier |
| OCDM | $\left(\frac{1}{2N}\sum_{i=0}^{2N-1}\bar{\gamma}^{-1}_{\mathrm{V},i}\right)^{-1}$ for all subchirps |
| SCCP | $\left(\frac{1}{2N}\sum_{i=0}^{2N-1}\bar{\gamma}^{-1}_{\mathrm{V},i}\right)^{-1}$ for the all subsymbols |
| OSDM | $\left(\frac{1}{\beta_k}\sum_{i=\nu_k-\lfloor\beta_k/2\rfloor}^{\nu_k+\lceil\beta_k/2\rceil-1}\bar{\gamma}^{-1}_{\mathrm{V},i}\right)^{-1}$ for the $k^{\mathrm{th}}$ tile |

# 4 PERFORMANCE ANALYSIS

Aiming to assess the usefulness of the proposed framework under a few distinct conditions, this chapter numerically analyzes the performance of OFDM, OCDM, SCCP, and OSDM when narrowband PLC channel is disturbed by the presence of the additive Gaussian noise. In this sense, it considers the violation of the CP length and the presence of STO to show the data communication scheme that delivers the best performance or is more resilient to the considered interference. The parameters used for performing the comparison between these data communication schemes are data rate and bit error probability. The data rate analysis is based on the UA and OA while the bit error probability analysis relies on the use of UA and adaptive modulation. A discussion about the numerical results obtained with the deduced closed-form expressions and the Monte Carlo simulation, which allows one to check the accuracy of the deduced closed-form expressions, are also detailed.

This chapter is organized as follows: Section 4.1 details the performance comparison and simulation parameters; Section 4.2 presents a comparison between the closed-form expressions-based and Monte Carlo simulations; Section 4.3 compares the three equalizers when only the closed-form expressions are considered; Section 4.4 presents the data rate results based on the closed-form expressions; and, finally, Section 4.5 presents the bit error probability results using the closed-form expressions.

## 4.1 SIMULATION PARAMETERS

To obtain the numerical results with the closed-form expressions, it is assumed that $L_h = 30$, $L_{cp} \in \{14, 21, 30\}$, $\Delta \in \{0, 5, 10\}$, $\Upsilon = 0$ dB for the data rate analysis, and the 16-QAM for the bit error probability analysis. As for the $\mathcal{B}$-geometry of the DOST, it is considered $\mathcal{B} = 64$. The PLC channel is generated following the channel model in [53] and considering the parameters found in [54, Annex D] with a frequency bandwidth of $B = 500$ kHz and $N = 256$. Those parameters can be found in Table 2.

Moreover, for the additive noise, it is utilized both the additive white and colored Gaussian noise models. With reference to the AWGN, the model considers a zero mean white Gaussian random process with a discrete power spectral density equal to $\mathcal{P}_{V_W,k} = N_0/2$, $k = 0, 1, ..., N-1$. While the ACGN model has a discrete power spectral density equal to $\mathcal{P}_{V_C,k} = \frac{\eta}{2} e^{(-\nu|\Delta f k|)} + \mathcal{P}_{V_W,k}$, $k = 0, 1, ..., N-1$, where the constants $\nu, \eta \in \mathbb{R}^+$ are equal to $1.2 \times 10^{-5}$ and $1.0 \times 10^{-15}$, respectively [55], and $\Delta f = B/N$. Table 3 summarizes the additive noise parameters.

For performing the data rate analysis based on OA and UA, the assumptions made concerning the channel model (i.e., filtered PLC channel disturbed by the presence of additive

Table 2 – Simulation parameters.

| **Parameters** | **Value** |
|---|---|
| $N$ | 256 |
| $B$ | 500 kHz |
| $L_h$ | 30 |
| $L_{cp}$ | $\{14, 21, 30\}$ |
| $\Delta$ | $\{0, 5, 10\}$ |
| $\Upsilon$ | 0 dB |
| $\mathcal{B}$ | 64 |

Table 3 – Additive noise parameters.

| **AWGN** | |
|---|---|
| **Parameters** | **Value** |
| $N_0$ | $8.16 \times 10^{-14}$ W |
| **ACGN** | |
| **Parameters** | **Value** |
| $v$ | $1.2 \times 10^{-5}$ |
| $\eta$ | $1.0 \times 10^{-15}$ |

and Gaussian random process) results in the following expression for the data rates [56]:

$$R = \frac{1}{2(2N + L_{cp})T_s} \sum_{k=0}^{2N-1} \log_2\left(1 + \frac{\tilde{\gamma}_k}{\Upsilon}\right), \tag{4.1}$$

where $\Upsilon$ is the gap factor from Shannon's capacity curve, $T_s$ is the sampling time, and $\tilde{\gamma}_k$ is the SNR of a given scheme (HS-OFDM, OCDM, SCCP, or OSDM).

Furthermore, the additive noise and interference are considered to be Gaussian random processes in all considered domains since the Central Limit Theorem applies in the transformation from the time domain to the frequency or Fresnel domains. Consequently, the bit error probability for the $M$-QAM constellation associated with the $k^{\text{th}}$ element (subcarrier, subchirp,

subsymbol or tile) is expressed as

$$P_{b,k} = \frac{4}{\log_2(M)} \left[ \left(1 - \frac{1}{\sqrt{M}}\right) Q\left(\sqrt{\frac{3}{M-1}\tilde{\gamma}_k}\right) - \left(1 - \frac{1}{\sqrt{M}}\right)^2 Q\left(\sqrt{\frac{3}{M-1}\tilde{\gamma}_k}\right)^2 \right] \tag{4.2}$$

with $M$ being the constellation order and $Q(\cdot)$ the Q-function. Furthermore, the average bit error probability, which will be used for performing bit error probability analysis, is given by

$$\overline{P}_b = \frac{1}{2N} \sum_{k=0}^{2N-1} P_{b,k}. \tag{4.3}$$

The data rate and error probability analyses are both in terms of the total transmission power (i.e, $R \times \mathcal{P}_T$ (dBm) and $\overline{P}_b \times \mathcal{P}_T$ (dBm)), which is expressed as

$$\begin{aligned} \mathcal{P}_T &= \sum_{k=0}^{2N-1} \tilde{\mathcal{P}}_{\mathrm{X},k,k} \\ &= \mathrm{tr}(\tilde{\boldsymbol{\mathcal{P}}}_{\mathrm{X}}), \end{aligned} \tag{4.4}$$

where $\mathrm{tr}(\cdot)$ is the trace operation, $\tilde{\boldsymbol{\mathcal{P}}}_{\mathrm{X}}$ is the signal power matrix related to the given scheme (HS-OFDM, OCDM, SCCP or OSDM). Depending on the CSI availability and the type of performance analysis, the total transmission power, $\mathcal{P}_T$, is differently allocated to the $2N$-block symbols. Note that the use of OA refers to the non-uniform allocation of $\mathcal{P}_T$ while the use of UA means that $\mathcal{P}_T$ is equally distributed.

## 4.2 CLOSED-FORM EXPRESSIONS AND MONTE CARLO SIMULATION COMPARISON

In this section, a comparison between the results obtained with the closed-form expressions and the Monte Carlo simulation is analyzed for the OCDM scheme. Similar analysis to other schemes is omitted because similar results are obtained with all of them. The numerical results calculated on the basis of the closed-form expressions of the OCDM scheme makes use of (4.2), while considering the SINR of the OCDM, is based on $\overline{P}_b \times \mathcal{P}_T$ (dBm) plots. In addition, the Monte Carlo simulation relies on the BER $\times \mathcal{P}_T$ (dBm) plots. As the lack of CSI at the transmitter is assumed, the use of UA together with adaptive modulation is considered. The adaptive modulation configuration is set to perform the 16-QAM constellation, the equalizer C-ZF is adopted, $L_{cp} = 14$, $\Delta = 5$, $\mathcal{P}_T \in [-10, 40]$ (dBm), and the PLC channel is corrupted by the presence of AWGN. For performing the Monte Carlo simulation, it is assumed the transmission of $10^7$ equiprobable $N$-block symbols, which are constituted by the points of a 16-QAM constellation, resulting in the transmission of $1.024 \times 10^{10}$ bits.

Figure 6 shows the numerical results for this comparison. As it can be seen, there is a perfect agreement between the numerical results outputted by the closed-form expressions

(i.e., the $\overline{P}_b$ curve) and Monte Carlo simulation (i.e., the BER curve). Also, it is observed that after a certain value of $\mathcal{P}_T$, its increase does not manage to improve the values of $\overline{P}_b$ and BER. This is an expected behavior because this simulation considers CP length violation and STO, causing the data communication system to operate under interference. Since the signal power and the interference are directly proportional with $\mathcal{P}_T$, the SINR will always have the interference increasing with the $\mathcal{P}_T$ resulting in $\overline{P}_b$ having a lower bound. Relying on the fact that numerical results obtained with the closed-form expressions and Monte Carlo simulation agree, the following sections present only the numerical results obtained with the closed-form expressions.

## 4.3 EQUALIZATION COMPARISON

This section presents a comparison between the frequency domain equalizers (i.e., C-ZF, M-ZF, and ST-ZF). To perform this comparison, it is adopted $\mathcal{P}_T \in [-10, 40]$ (dBm), the PLC channel corrupted by the presence of AWGN and ACGN, $L_{cp} = 14$, and $\Delta = 5$. Moreover, the UA technique is combined with the 16-QAM constellation. In contrast to Section 4.2, all data communication schemes are analyzed.

Figure 7 shows the attained results with C-ZF, M-ZF, and ST-ZF. The performance curves show that the C-ZF equalizer yields the best results, which is similar to what was reported in [51] for the OFDM scheme. For instance, while considering AWGN and $\mathcal{P}_T = 30$ dBm,

Figure 6 – Comparison between closed-form expressions of $\overline{P}_b$ and Monte Carlo simulation (BER) for the OCDM scheme while considering $L_{cp} = 14$, $\Delta = 5$, 16-QAM, and AWGN.

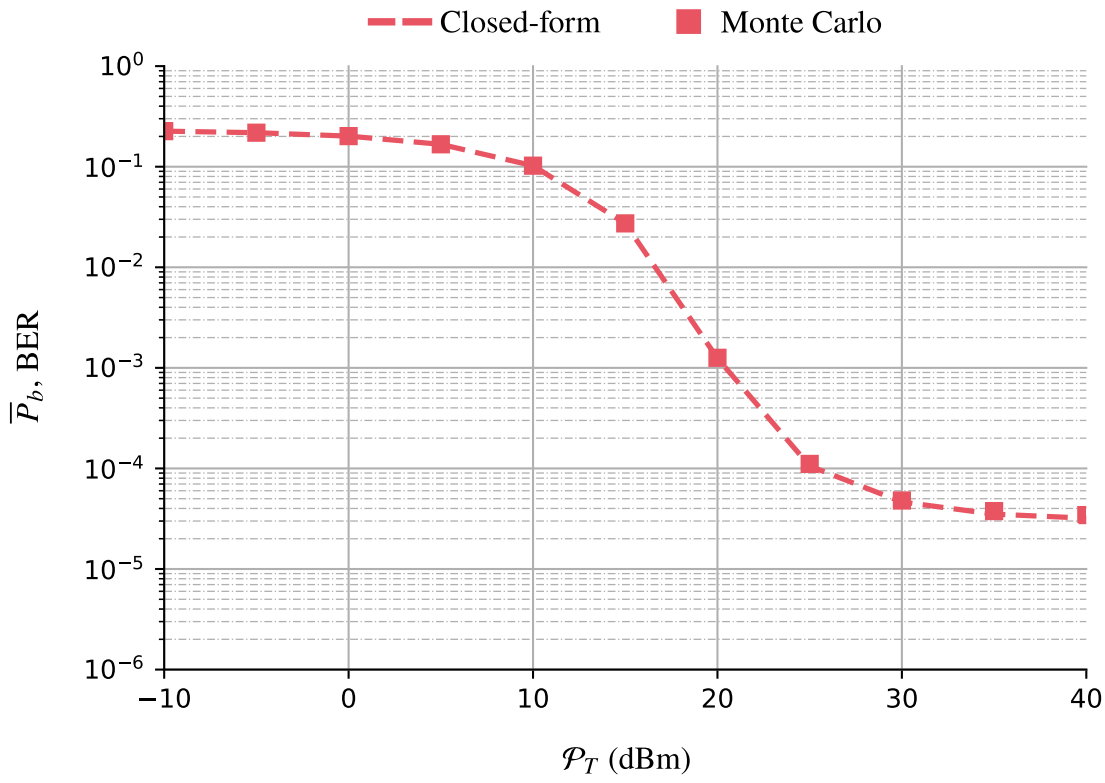

HS-OFDM reaches values of $\overline{P}_b$ equal to $4.50 \times 10^{-4}$,$1.05 \times 10^{-3}$, and $1.83 \times 10^{-3}$ when cosidering C-ZF, M-ZF, and ST-ZF, respectively. Similar results were found using other data communication schemes. Under the same noise disturbance, the OCDM obtains values of $\overline{P}_b$ equal to $4.64 \times 10^{-5}$ for the C-ZF, while the other equalizers, M-ZF and ST-ZF, yield $6.13 \times 10^{-4}$ and $1.79 \times 10^{-3}$, respectively. Also, for the SCCP, considering the C-ZF, the scheme reaches $\overline{P}_b = 9.20 \times 10^{-4}$, while the others equalizers attained higher values of $\overline{P}_b$. And for the last scheme, the OSDM achieves a value of $\overline{P}_b$ equal to $1.07 \times 10^{-3}$ for the C-ZF, $2.15 \times 10^{-3}$ for the M-ZF, and $3.36 \times 10^{-3}$ for the ST-ZF. Finally, similar behavior is also observed when ACGN is considered; however, with higher values of $\overline{P}_b$. All further numerical analyses regarding data rate and bit error probability in the following sections make use of the C-ZF, since it results in the best results among the equalizers considered in this thesis. Table 4 summarizes the results obtained in this section.

Table 4 – Values of $\overline{P}_b$ for $\mathcal{P}_T = 30$ dBm when the equalizers C-ZF, M-ZF, and ST-ZF are applied to PLC channel corrupted by AWGN.

| **Scheme** | **C-ZF** | **M-ZF** | **ST-ZF** |
|---|---|---|---|
| HS-OFDM | $4.50 \times 10^{-4}$ | $1.05 \times 10^{-3}$ | $1.83 \times 10^{-3}$ |
| OCDM | $4.64 \times 10^{-5}$ | $6.13 \times 10^{-4}$ | $1.79 \times 10^{-3}$ |
| SCCP | $9.20 \times 10^{-4}$ | $1.18 \times 10^{-3}$ | $3.06 \times 10^{-3}$ |
| OSDM | $1.07 \times 10^{-3}$ | $2.15 \times 10^{-3}$ | $3.36 \times 10^{-3}$ |

## 4.4 DATA RATE COMPARISON

This section discusses the performance in terms of data rates when UA and OA are considered. The use of OA means that the transmitter knows the CSI and uses the waterfilling algorithm to allocate distinct amounts of power to each subcarrier, subshirps, subsymbols, or tiles when it is utilized HS-OFDM, OCDM, SCCP, or OSDM, respectively. On the other hand, UA means that the CSI is not available at the transmitter side and the total transmission power is equally distributed among subcarriers, subchirps, subsymbols, and tiles when it is utilized HS-OFDM, OCDM, SCCP, or OSDM, respectively. Note that the nSNR value for the OCDM and SCCP are the same for all subchirps and subsymbols, meaning the total transmission power is equally distributed among subchirps and subsymbols regardless of the power allocation technique considered.

The simulation results displayed in terms of $R$ (Mbps) $\times$ $\mathcal{P}_T$ (dBm), while adopting UA, are illustrated in Figure 8. First, for the simulations without any form of interference ($L_{cp} = 30$ and $\Delta = 0$), the HS-OFDM provides a better $R$ than the other schemes through all values of $\mathcal{P}_T$ and noise types considered. Regarding $\mathcal{P}_T = 30$ dBm, the HS-OFDM yields $R$ equal to 5 and 4.22 Mbps for the AWGN and ACGN, respectively, while the OSDM provides the second best

performance of data rate, achieving values of $R$ equal to 4.67 and 3.96 Mbps. Also, both the OCDM and SCCP yield 4.26 Mbps and 3.71 Mbps for the aforementioned additive noises. It is important to highlight that the OCDM and SCCP, when using $L_{cp} = 30$ and $\Delta = 0$, achieve the same performance because their nSNRs are exactly the same.

Moreover, Figure 8 shows that as the interference starts to grow, the OSDM and SCCP have proven to be more resilient to data rate loss due to CP length violation and STO among the four data communication schemes, while the OCDM is the third most resilient. Indeed, as an example, for $\mathcal{P}_T = 30$ dBm, $L_{cp} = 21$, and ACGN, the data rate of the OSDM drops from 4 to 3.86 Mbps as $\Delta$ increases from 0 to 10 and the data rates of the SCCP drops from 3.75 to 3.57 Mbps. While, the OCDM decreases from 3.75 to 3.43 Mbps and the HS-OFDM from 4.26 to 3.78. To summarize, even though the HS-OFDM is more fragile to the interference than the others, it yields better data rate results for most of the considered $\mathcal{P}_T$ interval in comparison to the other data communication schemes. Indeed, the HS-OFDM only loses in performance to the OSDM when considering the high values of $\mathcal{P}_T$, which is when the interference starts to compromise more the data rate performance of the HS-OFDM than the OSDM. For instance, with $L_{cp} = 14$ (i.e., a strong CP length violation), the HS-OFDM still generates better data rate results among the four data communication schemes for the values of $\mathcal{P}_T \leq 25$ dBm and under the presence of both additive noises (i.e., AWGN and ACGN). To put into numbers, when $\mathcal{P}_T = 20$ dBm, $\Delta = 10$, and AWGN, the HS-OFDM yields $R$ close to 3.24 Mbps, the OCDM attains $R = 2.67$ Mpbs, the SCCP yields 2.70 Mbps, and the OSDM attains $R = 3.11$ Mbps.

The performance comparison in terms of $R$ (Mbps) $\times$ $\mathcal{P}_T$ (dBm) while considering OA and comparing it to the UA are shown in Figure 9. First, since the transmitter must know the CSI to perform the OA through the waterfilling algorithm, the numerical simulations contemplate only the cases with $L_{cp} = 30$ and $\Delta \in \{0, 5, 10\}$. Therefore, the nSNRs used to perform the power allocation are described in Table 1, since it is assumed that the transmitter does not have knowledge about any kind of interference present in the data communication system. In these plots is clear that the OCDM and SCCP attain the same performance for both allocation techniques because of their nSNR characteristic. In contrast, the HS-OFDM and OSDM with OA offer much better data rates than with UA when the total transmission power is low (e.g., $\mathcal{P}_T$ interval of $-20$ to 0 dBm for AWGN and $-15$ to 5 dBm for ACGN). For example, while considering AWGN and $\Delta = 10$, the HS-OFDM reaches a value of $R = 0.27$ Mbps when adopting $\mathcal{P}_T$ equal to $-11$ and $-8$ dBm with OA and UA, respectively. On the other hand, the OSDM requires bigger values of $\mathcal{P}_T$ than the HS-OFDM to achieve the same $R$, reaching a data rate equal to 0.27 Mbps when $\mathcal{P}_T = -10$ dBm with OA and $\mathcal{P}_T = -6$ dBm with UA. Moreover, in a certain interval of $\mathcal{P}_T$, the data rate stop starts to saturate due to the interference, reaching an upper bound. That interval is, approximately, $\mathcal{P}_T \geq 15$ and $\mathcal{P}_T \geq 20$ dBm for AWGN and ACGN, respectively, and this interval is further away from the one that OA really improves the data rate. Therefore, the use of OA benefits the data rate performance even in the presence of interference caused by STO.

Therefore, the HS-OFDM presents the best result of $R$ for all values of $\mathcal{P}_T$ considered in this thesis in most cases. The exceptions are as follows:

- The HS-OFDM with UA yields lower values of $R$ than the OSDM with OA in the interval of $-20 \leq \mathcal{P}_T \leq -5$ and $-20 \leq \mathcal{P}_T \leq -10$ dBm for AWGN and ACGN, respectively.
- In the high values of $\mathcal{P}_T$ considered in this study ($\mathcal{P}_T \geq 20$ dBm), the HS-OFDM does not obtain the best data rate because its low resilience to the CP length violation and STO.

However, these cases do not seem to be enough to discard the HS-OFDM as the obvious choice to use when the CSI is available at the transmitter side.

Figure 7 – Comparison between the equalizers C-ZF, M-ZF, and ST-ZF in terms of $\overline{P}_b \times \mathcal{P}_T$ (dBm) for the OCDM, HS-OFDM, SCCP, and OSDM when $L_{cp} = 14$, $\Delta = 5$, 16-QAM, and both types of additive noise are considered.

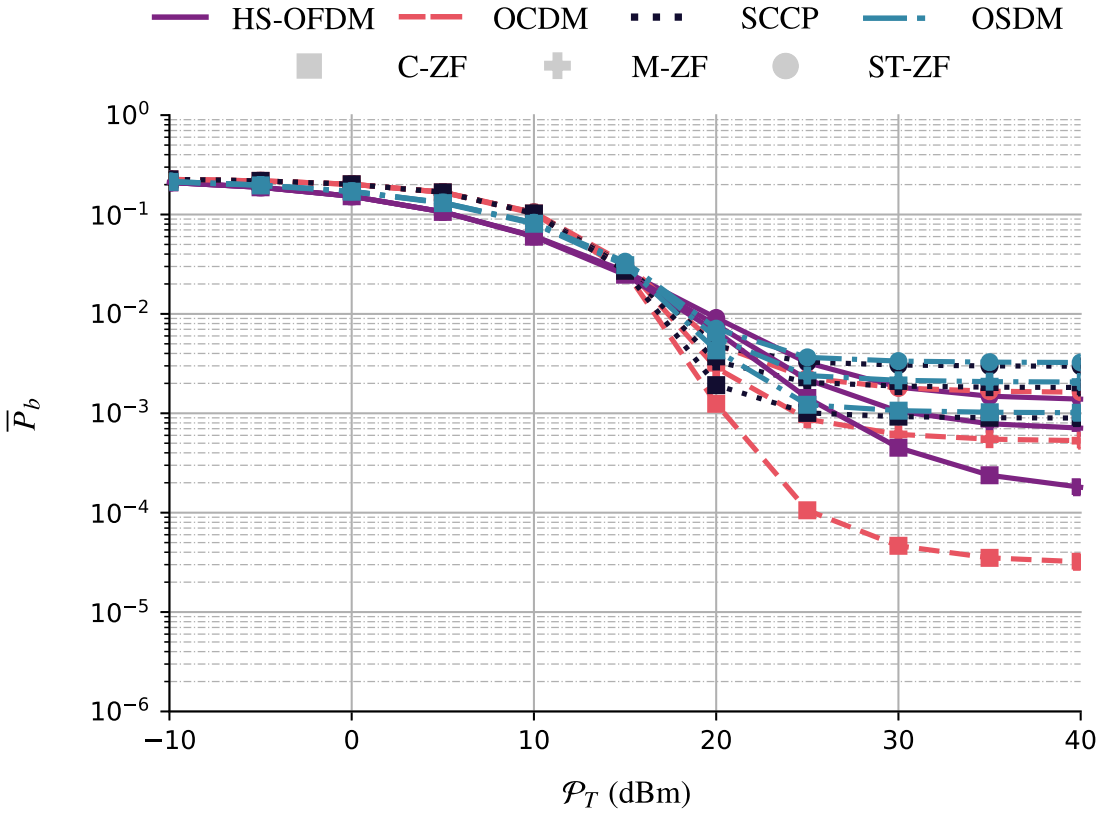


(a) AWGN

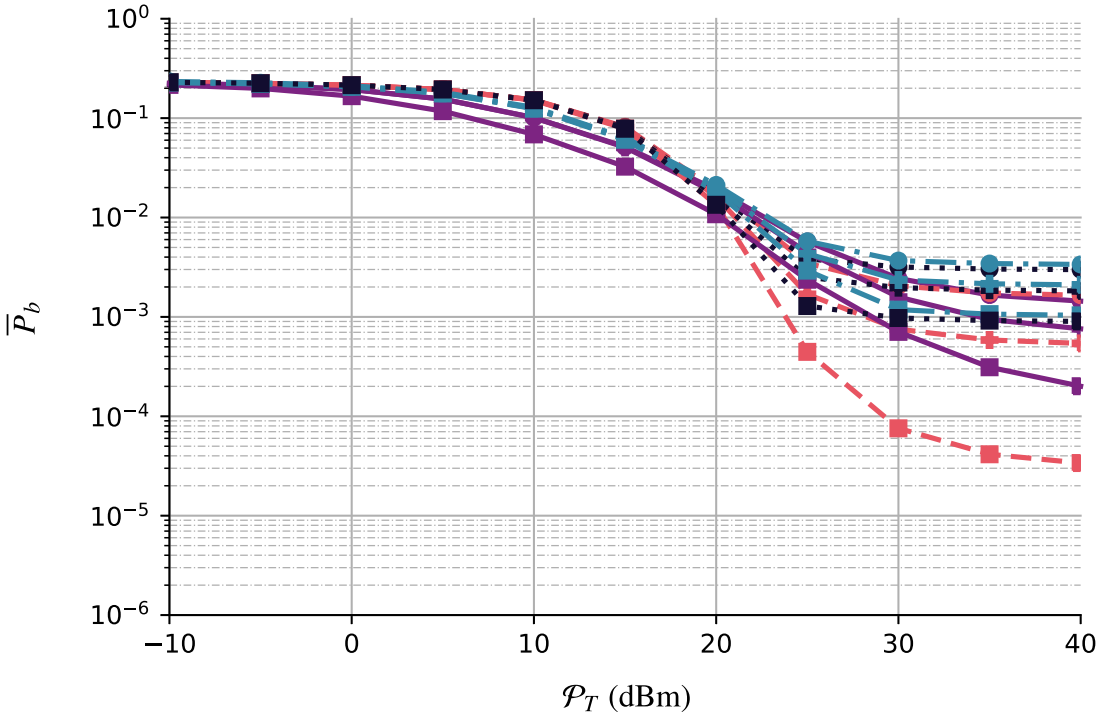


(b) ACGN

Figure 8 – $R$ (Mbps) $\times \mathcal{P}_T$ (dBm) for the HS-OFDM, OCDM, SCCP, and OSDM, when $L_{cp} \in \{14, 21, 30\}$, $\Delta \in \{0, 5, 10\}$, and both types of additive noise are considered.

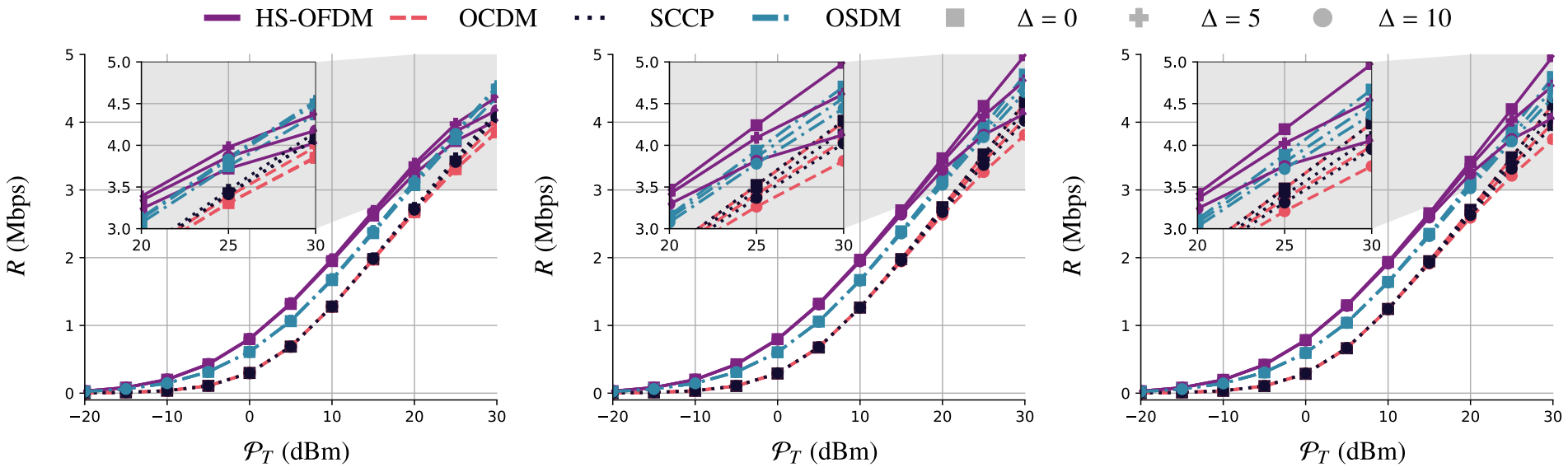


(a) $L_{cp} = 14$ and AWGN

(b) $L_{cp} = 21$ and AWGN

(c) $L_{cp} = 30$ and AWGN

(d) $L_{cp} = 14$ and ACGN

(e) $L_{cp} = 21$ and ACGN

(f) $L_{cp} = 30$ and ACGN

Figure 9 – $R$ (Mpbs) $\times \mathcal{P}_T$ (dBm) for the HS-OFDM, OCDM, SCCP, and OSDM schemes while considering $L_{cp} = 30$, $\Delta \in \{0, 5, 10\}$, and both types of additive noise.

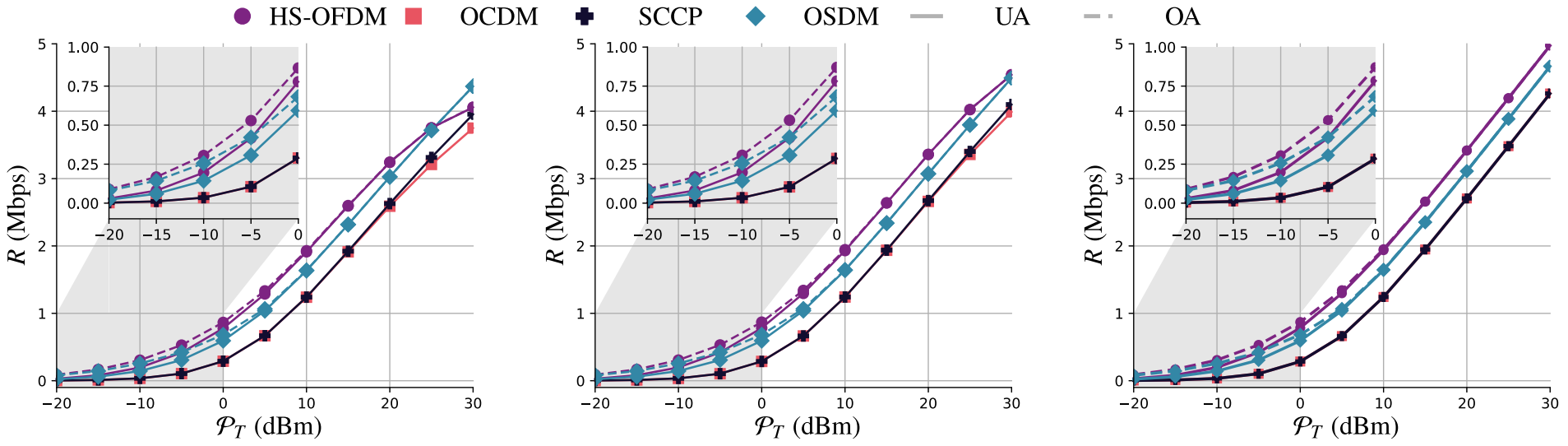


(a) $\Delta = 10$ and AWGN

(b) $\Delta = 5$ and AWGN

(c) $\Delta = 0$ and AWGN

(d) $\Delta = 10$ and ACGN

(e) $\Delta = 5$ and ACGN

(f) $\Delta = 0$ and ACGN

Figure 10 – $\overline{P}_b \times \mathcal{P}_T$ (dBm) for the HS-OFDM, OCDM, SCCP, and OSDM, when it is consider $L_{cp} \in \{14, 21, 30\}$, $\Delta \in \{0, 5, 10\}$, 16-QAM and both types of additive noise.

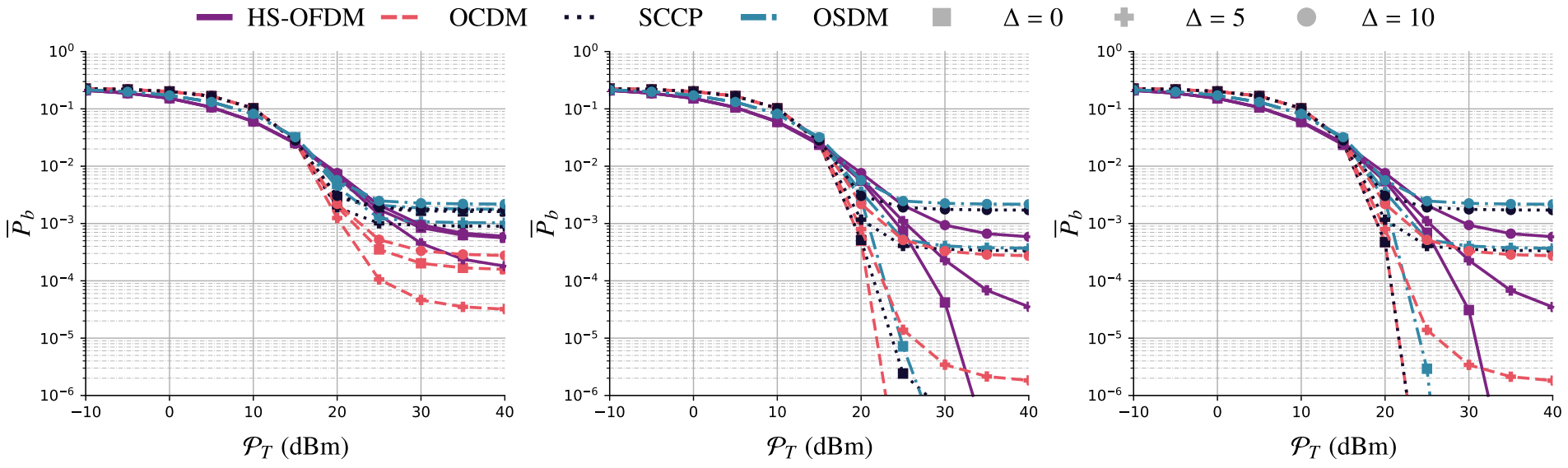


(a) $L_{cp} = 14$ and AWGN (b) $L_{cp} = 21$ and AWGN (c) $L_{cp} = 30$ and AWGN

(d) $L_{cp} = 14$ and ACGN (e) $L_{cp} = 21$ and ACGN (f) $L_{cp} = 30$ and ACGN

## 4.5 BIT ERROR PROBABILITY

This section focuses on the performance analysis in terms of bit error probability when the 16-QAM constellation is used to transmit data (adaptive modulation). In other words, the CSI is not available at the transmitter side, and, as a consequence, subcarriers, subchirps, subsymbols, and tiles transmit the same integer number of bits, which is equal to $b = \log_2 16 = 4$. Note that this performance analysis is different from the analysis based on the use of UA since the latter allocates a real number of bits in accord with the nSNR, which is not what adaptive modulation advocates.

Figure 10 displays the graphs of $\overline{P}_b \times \mathcal{P}_T$ (dBm) while considering $L_{cp} \in \{14, 21, 30\}$ and $\Delta \in \{0, 5, 10\}$. When considering the system operating under AWGN, $L_{cp} = 30$, and $\Delta = 0$ are considered, the HS-OFDM and OSDM yield $\overline{P}_b = 10^{-6}$ when the $\mathcal{P}_T$ is equal to 32 and 25 dBm, respectively, while the OCDM and SCCP only require $\mathcal{P}_T = 22$ dBm to achieve the aforementioned value of $\overline{P}_b$. It is important to note that the curves of $\overline{P}_b \times \mathcal{P}_T$ for the OCDM and SCCP are exactly the same in the absence of interference provoked by the CP violation and STO since their nSNRs are equal.

Also, as the value of $L_{cp}$ decreases and $\Delta$ increases, the interference starts rising substantially. Consequently, the performance of all data communication schemes decrease. For example, for the simulations $L_{cp} = 21$ and AWGN, to achieve a $\overline{P}_b = 10^{-4}$, the HS-OFDM requires values of $\mathcal{P}_T$ equal to 29 and 32 dBm for $\Delta$ equal to 0 and 5, respectively. For the OCDM scheme, one can see that this data communication scheme generates the aforementioned $\overline{P}_b$ when $\mathcal{P}_T$ is equal to 21 and 23 dBm for $\Delta$ equal to 0 and 5, respectively. Moreover, the OSDM and SCCP are proven to be the data communication schemes which are most affected with the increasing interference, since only with $\Delta$ equal to 0 and $\mathcal{P}_T$ equal to 23 dBm for the OSDM and 22 dBm for the SCCP they achieve $\overline{P}_b = 10^{-4}$.

Furthermore, for $L_{cp} = 14$, the OCDM continues to yield better values of $\overline{P}_b$ than the other data communication schemes, being the only one among them to reach values of $\overline{P}_b$ lower than $3.3 \times 10^{-4}$ for all $\Delta$ considered. In this sense, the OCDM showed better resistance to performance loss in terms of $\overline{P}_b$ than the other data communication schemes as the interference increases. In counterpart, the SCCP and OSDM are the most fragile to interference in terms of $\overline{P}_b$. Indeed, the SCCP fragility to interference in terms of $\overline{P}_b$ is very interesting, since its SNR is equal to the OCDM, which is the most resilient among the considered data communication schemes. Thus, leading to the conclusion that CSS-based data communication scheme is less impacted than the others regarding the interference caused by the CP length violation and STO.

For the numerical simulations considering ACGN, all data communication schemes behave similarly to the simulations with AWGN as $L_{cp}$, $\Delta$, and $\mathcal{P}_T$ vary. However, all data communication schemes when operating over PLC channels corrupted by ACGN require more total transmission power than when operating over PLC channels corrupted by AWGN to yield

the same $\overline{P}_b$. For instance, with $L_{cp} = 21$ and $\Delta = 0$, to achieve $\overline{P}_b = 10^{-6}$, the OCDM requires $\mathcal{P}_T$ equal to 23 and 27 dBm for AWGN and ACGN, respectively. Meanwhile, the HS-OFDM requires 33 and 37 dBm, the SCCP 28 and 31 dBm, and the OSDM 27 and 32 dBm for those same types of additive noise.

To summarize, the OCDM displays the best results when there is no interference, requiring almost 10 dBm less of the total power transmission to reach $\overline{P}_b = 10^{-6}$ than the HS-OFDM and 3 dBm less than the OSDM. And, even though the SCCP attains the same curve of $\overline{P}_b \times \mathcal{P}_T$ (dBm) than the OCDM without interference, the SCCP performance presents significant degradation in the presence of increasing interference. Consequently, the OCDM is the better choice between the four presented data communication schemes when adaptive modulation applies. Indeed, it shows better performance in terms of $\overline{P}_b \times \mathcal{P}_T$ (dBm) even in the presence of interference due to CP length violation and STO. Thus, making the OCDM the best option to use when the adaptive modulation applies, which characterize a scenario where CSI is not available. However, if the computational complexity is one of the biggest concern and the interference is weak, the SCCP is more suitable candidate to perform the data communication.

# 5 CONCLUSION

This thesis has advanced the investigation of the interference caused by the CP length violation and STO in a set of data communication schemes, which are implemented by using DFT, applied to PLC systems. In this sense, it has discussed a framework to merge the set of data communication scheme into a general formulation. Relying on the proposed framework, this thesis has advanced closed-form expressions for quantifying the interference caused by the CP length violation and STO. In the sequel, it has qualitatively shown the usefulness of such expressions for carrying out performance comparisons between the data communication schemes. Moreover, it has quantitatively assessed performances in terms of data rate and bit error probability to find the conditions in which each data communication scheme can be more suitable.

Regarding the proposed framework, it has shown that it allows the unification of HS-OFDM, OCDM, SCCP, and OSDM into a set of data communication schemes in which the DFT is the core tool. In fact, by changing one of the parameters of the proposed formulation, it is possible to derive the HS-OFDM, OCDM, SCCP, and OSDM schemes. Consequently, it facilitates the switching between these data communication schemes when it is necessary to carry out a broad change in the PHY layer in order to adapt to the changing channel conditions and the availability of CSI at the transmitter side. Moreover, this thesis has advanced the formulation presented in [50, 51] to deduce closed-form expressions of the OCDM, SCCP, and OSDM for the estimated symbol, SINR, and SNR when the additive noise is a white or colored Gaussian random process. Consequently, it has detailed data rate and bit error probability performance comparisons among HS-OFDM, OCDM, SCCP, and OSDM under distinct levels of the CP length violation and STO. Based on the availability of the CSI at the transmitter side, the suitability of HS-OFDM, OCDM, SCCP, and OSDM has been discussed. Moreover, it was demonstrated that the nSNRs of the OCDM, SCCP, and OSDM are equal to the harmonic mean of the HS-OFDM's nSNR, which emphasizes the existing relationship among them. Consequently, their combined use in a software-defined PLC system, in which the data communication schemes can be dynamically selected to meet a specific goal, can be considered.

Numerical simulations have proven the consistency of the deduced closed-form expressions for evaluating data rates and bit error probabilities and comparing the results outputted by the Monte Carlo simulation when CP length violation and STO are considered. Moreover, the data rate analysis, in which the performance of UA and OA are compared, and bit error probabilities using adaptive modulation has provided valuable insights about the HS-OFDM, OCDM, SCCP, and OSDM. The analysis has considered PLC system modeled as a linear and time-invariant PLC channel corrupted by additive noises modeled as AWGN and ACGN and the interference caused by the CP length violation and STO. The numerical results show that the HS-OFDM scheme attains the highest data rate for most values of the total transmission power even in the presence of interference and considering both power allocation techniques. The

OSDM scheme offers the second-best data rate performance. Indeed, under specific scenarios, such as high values of the total transmission power together with the presence of interference, the OSDM can compete with the HS-OFDM.

Regarding the performance analysis in terms of bit error probabilities, the numerical analysis has shown that the lack of CSI at the transmitter side imposes the use of the adaptive modulation. In this scenario, the OCDM is the data communication that offers the best bit error probability values in comparison to HS-OFDM, SCCP, and OSDM for the considered interval of the total transmission power. Also, the bit error probabilities of the OCDM and SCCP tend to be the same in the absence of the CP length violation and STO; however, the OCDM offers improved bit error probability as these problems become significant. In addition, the SCCP and OSDM are almost equally degraded under strong interference. In the scenario with mild interference, the HS-OFDM offers the second-best performance.

Overall, if the aim is to maximize data rate, which imposes CSI availability at the transmitter side, then the best option is the HS-OFDM followed by the OSDM. However, if adaptive modulation is adopted, which implies the CSI being unavailable at the transmitter side, the best option is the OCDM. The second best schemes are the SCCP if the interference is absent or weak and the HS-OFDM if mild or strong interference corrupts the data communication system.

## 5.1 FUTURE WORK

The future work are listed as follow:

- The extend the formulation to address the interference caused by clock offset, frequency offset, and degraded channel estimation when both baseband and passband are considered.
- The investigation of code-division multiple access (CDMA) on data communication schemes such as the OCDM and OSDM and perform a comparison with the well-established multicarrier CDMA schemes.
- The investigation of the proposed framework for analyzing the performance of hybrid communication systems, which combine power line and wireless communications, when the OFDM, OCDM, SCCP, and OSDM applies.

# REFERENCES


[1] D. Minoli, K. Sohraby, and B. Occhiogrosso, "IoT considerations, requirements, and architectures for smart buildings—energy optimization and next-generation building management systems," *IEEE Internet of Things Journal*, vol. 4, no. 1, pp. 269–283, 2017.

[2] L. de M. B. A. Dib, V. Fernandes, M. de L. Filomeno, and M. V. Ribeiro, "Hybrid PLC/wireless communication for smart grids and internet of things applications," *IEEE Internet of Things Journal*, vol. 5, no. 2, pp. 655–667, 2018.

[3] S. Galli, A. Scaglione, and Z. Wang, "For the grid and through the grid: The role of power line communications in the smart grid," *Proceedings of the IEEE*, vol. 99, no. 6, pp. 998–1027, 2011.

[4] M. Wollschlaeger, T. Sauter, and J. Jasperneite, "The future of industrial communication: Automation networks in the era of the internet of things and industry 4.0," *IEEE Industrial Electronics Magazine*, vol. 11, no. 1, pp. 17–27, 2017.

[5] R. M. de Oliveira, A. B. Vieira, H. A. Latchman, and M. V. Ribeiro, "Medium access control protocols for power line communication: A survey," *IEEE Communications Surveys Tutorials*, vol. 21, no. 1, pp. 920–939, 2019.

[6] G. Huang, D. Akopian, and C. L. P. Chen, "Measurement and characterization of channel delays for broadband power line communications," *IEEE Transactions on Instrumentation and Measurement*, vol. 63, no. 11, pp. 2583–2590, 2014.

[7] T. R. de Oliveira, C. A. Marques, W. A. Finamore, S. L. Netto, and M. V. Ribeiro, "A methodology for estimating frequency responses of electric power grids," *Journal of Control, Automation and Electrical Systems*, vol. 25, no. 6, pp. 720–731, 2014.

[8] T. R. de Oliveira, A. A. M. Picorone, S. L. Netto, and M. V. Ribeiro, "Characterization of Brazilian in-home power line channels for data communication," *Electric Power Systems Research*, vol. 150, pp. 188–197, 2017.

[9] L. G. da S. Costa, G. R. Colen, A. C. M. de Queiroz, V. L. R. da Costa, U. R. C. Vitor, F. V. dos Santos, and M. V. Ribeiro, "Access impedance in brazilian in-home, broadband and low-voltage electric power grids," *Electric power systems research*, vol. 171, pp. 141–149, 2019.

[10] L. G. da S. Costa, A. Queiroz, V. Costa, and M. Ribeiro, "An analog filter bank-based circuit for performing the adaptive impedance matching in PLC systems," *Journal of Communication and Information Systems*, vol. 36, no. 1, pp. 133–150, Aug. 2021.

[11] A. A. M. Picorone, T. R. de Oliveira, R. Sampaio-Neto, M. Khosravy, and M. V. Ribeiro, "Channel characterization of low voltage electric power distribution networks for PLC applications based on measurement campaign," *International Journal of Electrical Power & Energy Systems*, vol. 116, p. 105554, 2020.

[12] T. F. do A. Nogueira, G. R. Colen, V. Fernandes, and M. V. Ribeiro, "Statistical modeling of magnitudes of Brazilian in-home PLC and hybrid PLC-wireless channels," *Physical Communication*, vol. 39, p. 101014, 2020.

[13] M. Ribeiro, C. Duque, and J. Romano, "An interconnected type-1 fuzzy algorithm for impulsive noise cancellation in multicarrier-based power line communication systems," *IEEE Journal on Selected Areas in Communications*, vol. 24, no. 7, pp. 1364–1376, 2006.

[14] L. G. Oliveira, G. R. Colen, A. J. Han Vinck, and M. V. Ribeiro, "Resource allocation in HS-OFDM-based PLC systems: A tutorial," *Journal of Communication and Information Systems*, vol. 33, no. 1, 2018.

[15] M. V. Ribeiro, G. R. Colen, F. V. de Campos, Z. Quan, and H. V. Poor, "Clustered-orthogonal frequency division multiplexing for power line communication: When is it beneficial?" *IET Communications*, vol. 8, no. 13, pp. 2336–2347, 2014.

[16] H. Zou, S. Jagannathan, and J. M. Cioffi, "Multiuser OFDMA resource allocation algorithms for in-home power-line Communications," in *IEEE Global Telecommunications Conference*, 2008, pp. 1–5.

[17] N. Papandreou and T. Antonakopoulos, "Resource allocation management for indoor power-line communications systems," *IEEE Transactions on Power Delivery*, vol. 22, no. 2, pp. 893–903, 2007.

[18] G. R. Colen, L. G. de Oliveira, A. J. H. Vinck, and M. V. Ribeiro, "A spectral compressive resource allocation technique for PLC systems," *IEEE Transactions on Communications*, vol. 65, no. 2, pp. 816–826, 2017.

[19] G. R. Colen, H. Schettino, D. Fernandes, L. M. Sirimarco, F. P. de Campos, W. A. Finamore, H. A. Latchman, and M. V. Ribeiro, "A temporal compressive resource allocation technique for complexity reduction in PLC transceivers," *Transactions on Emerging Telecommunications Technologies*, vol. 28, no. 2, p. e2951, 2017.

[20] G. R. Colen, L. G. de Oliveira, C. B. Zeller, A. Han Vinck, and M. V. Ribeiro, "Statistical analysis and modeling of a novel parameter for resource allocation in multicarrier PLC systems," *Transactions on Emerging Telecommunications Technologies*, vol. 28, no. 11, p. e3180, 2017.

[21] Y. Coutinho, G. Colen, and M. Ribeiro, "An enhanced temporal compressive resource allocation technique for PLC systems," in *XXXVIII Simpósio Brasileiro de Telecomunicações e Processamento de Sinais*, 11 2020, pp. 1–5.

[22] R. M. Oliveira, L. G. de Oliveira, A. B. Vieira, and M. V. Ribeiro, "An enhanced cooperative mac protocol for hybrid plc/wireless systems," *Computer Networks*, vol. 163, p. 106878, 2019.

[23] M. de L. Filomeno, M. L. R. de Campos, H. V. Poor, and M. V. Ribeiro, "Hybrid power line/wireless systems: Power allocation for minimizing the average bit error probability," *IEEE Transactions on Communications*, pp. 1–12, Dec. 2021, early access, doi: 10.1109/TCOMM.2021.3139326.

[24] M. de L. Filomeno, M. L. R. de Campos, H. V. Poor, and M. V. Ribeiro, "Hybrid power line/wireless systems: An optimal power allocation perspective," *IEEE Transactions on Wireless Communications*, vol. 19, no. 10, pp. 6289–6300, 2020.

[25] S. Baig, H. Muhammad Asif, T. Umer, S. Mumtaz, M. Shafiq, and J.-G. Choi, "High data rate discrete wavelet transform-based PLC-VLC design for 5G communication systems," *IEEE Access*, vol. 6, pp. 52 490–52 499, 2018.

[26] Y. H. Ng and T. C. Chuah, "Single-carrier cyclic prefix-assisted PLC systems with frequency-domain equalization for high-data-rate transmission," *IEEE Transactions on Power Delivery*, vol. 25, no. 3, pp. 1450–1457, 2010.

[27] F. A. La-Gatta, M. V. Ribeiro, A. P. Legg, and R. Machado, "Coded CP-SC communication scheme for outdoor power line communications," in *IEEE International Symposium on Power Line Communications and its Applications*, 2010, pp. 160–165.

[28] G. R. Colen and M. V. Ribeiro, "A flexible multicarrier scheme based on the discrete orthogonal Stockwell transform," *IEEE Systems Journal*, vol. 14, no. 4, pp. 5284–5295, 2020.

[29] R. Stockwell, "A basis for efficient representation of the S-transform," *Digital Signal Processing*, vol. 17, no. 1, pp. 371–393, 2007.

[30] Y. Wang, "Efficient Stockwell transform with applications to image processing," PhD. dissertation, Dept. Applied Math., University of Waterloo, Waterloo, ON, Canada, 2011.

[31] Y. Wang and J. Orchard, "Fast discrete orthonormal Stockwell transform," *SIAM Journal on Scientific Computing*, vol. 31, no. 5, pp. 4000–4012, 2009.

[32] Y. Wang and J. Orchard, "On the use of the Stockwell transform for image compression," in *Image Processing: Algorithms and Systems VII*, vol. 7245, International Society for Optics and Photonics. SPIE, 2009, pp. 33–39.

[33] Y. Wang and J. Orchard, "The discrete orthonormal Stockwell transform for image restoration," in *16th IEEE International Conference on Image Processing*, 2009, pp. 2761–2764.

[34] B. Nithya, Y. B. Sankari, K. Manikantan, and S. Ramachandran, "Discrete orthonormal Stockwell transform based feature extraction for pose invariant face recognition," *Procedia Computer Science*, vol. 45, pp. 290–299, 2015, international Conference on Advanced Computing Technologies and Applications (ICACTA).

[35] X. Ouyang and J. Zhao, "Orthogonal chirp division multiplexing," *IEEE Transactions on Communications*, vol. 64, no. 9, pp. 3946–3957, 2016.

[36] X. Ouyang and J. Zhao, "Orthogonal chirp division multiplexing for coherent optical fiber communications," *Journal of Lightwave Technology*, vol. 34, no. 18, pp. 4376–4386, 2016.

[37] X. Ouyang, G. Talli, M. Power, and P. Townsend, "Orthogonal chirp-division multiplexing for IM/DD-based short-reach systems," *Optics Express*, vol. 27, no. 16, pp. 23 620–23 632, Aug 2019.

[38] R. Bomfin, M. Chafii, and G. Fettweis, "Performance assessment of orthogonal chirp division multiplexing in MIMO space time coding," in *IEEE 2nd 5G World Forum*, 2019, pp. 220–225.

[39] P.-J. Bouvet, Y. Auffret, and C. Aubry, "On the analysis of orthogonal chirp division multiplexing for shallow water underwater acoustic communication," in *OCEANS 2017 - Aberdeen*, 2017, pp. 1–5.

[40] P. Zhu, X. Xu, X. Tu, Y. Chen, and Y. Tao, "Anti-multipath orthogonal chirp division multiplexing for underwater acoustic communication," *IEEE Access*, vol. 8, pp. 13 305–13 314, 2020.

[41] X. Ouyang, O. A. Dobre, Y. L. Guan, and J. Zhao, "Chirp spread spectrum toward the Nyquist signaling rate—orthogonality condition and applications," *IEEE Signal Processing Letters*, vol. 24, no. 10, pp. 1488–1492, 2017.

[42] M. S. Omar and X. Ma, "Spectrum design for orthogonal chirp division multiplexing transmissions," *IEEE Wireless Communications Letters*, vol. 9, no. 11, pp. 1990–1994, 2020.

[43] L. G. de Oliveira, M. B. Alabd, B. Nuss, and T. Zwick, "An OCDM Radar-Communication System," in *14th European Conference on Antennas and Propagation*, 2020, pp. 1–5.

[44] L. G. de Oliveira, B. Nuss, M. B. Alabd, Y. Li, L. Yu, and T. Zwick, "MIMO-OCDM-based joint radar sensing and communication," in *15th European Conference on Antennas and Propagation*, 2021, pp. 1–5.

[45] L. G. Oliveira, M. de L. Filomeno, H. V. Poor, and M. V. Ribeiro, "Orthogonal chirp-division multiplexing for power line sensing via time-domain reflectometry," *IEEE Sensors Journal*, vol. 21, no. 2, pp. 955–964, 2021.

[46] X. Ouyang, O. A. Dobre, and J. Zhao, "Unbiased channel estimation based on the discrete Fresnel transform for CO-OFDM Systems," *IEEE Photonics Technology Letters*, vol. 29, no. 8, pp. 691–694, 2017.

[47] X. Ouyang, C. Antony, G. Talli, and P. D. Townsend, "Robust channel estimation for coherent optical orthogonal chirp-division multiplexing with pulse compression and noise rejection," *Journal of Lightwave Technology*, vol. 36, no. 23, pp. 5600–5610, 2018.

[48] M. S. Omar and X. Ma, "Performance analysis of OCDM for wireless communications," *IEEE Transactions on Wireless Communications*, vol. 20, no. 7, pp. 4032–4043, 2021.

[49] L. de M. B. A. Dib, G. R. Colen, M. de L. Filomeno, and M. V. Ribeiro, "Orthogonal chirp division multiplexing for baseband data communication systems," *IEEE Systems Journal*, vol. 14, no. 2, pp. 2164–2174, 2020.

[50] W. A. Martins, F. Cruz–Roldán, M. Moonen, and P. S. Ramirez Diniz, "Intersymbol and intercarrier interference in OFDM transmissions through highly dispersive channels," in *27th European Signal Processing Conference*, 2019, pp. 1–5.

[51] J. I. Montojo and L. B. Milstein, "Effects of imperfections on the performance of OFDM systems," *IEEE Transactions on Communications*, vol. 57, no. 7, pp. 2060–2070, 2009.

[52] T. F. Moreira, A. Camponogara, S. Baig, and M. V. Ribeiro, "Data rate and bit error probability in narrowband PLC systems: OCDM versus HS-OFDM," in *XXXIX Simpósio Brasileiro de Telecomunicações e Processamento de Sinais*, 2021, pp. 1–5.

[53] M. Zimmerman and K. Dostert, "A multipath model for the power line channel," *IEEE Transactions on Communications*, vol. 50, no. 4, pp. 553–559, Apr. 2002.

[54] *IEEE Standard for low frequency (less than 500 kHz) narrow band power line communication for smart grid application*, IEEE Std. 1901.2, Dec. 2013.

[55] M. Katayama, T. Yamazato, and H. Okada, "A mathematical model of noise in narrowband power line communication systems," *IEEE Journal on Selected Areas in Communication*, vol. 24, no. 7, pp. 1267–1276, Jul. 2006.

[56] T. M. Cover and J. A. Thomas, *Elements of Information Theory*. Wiley-Interscience, Jul, 2006.

[57] X. Ouyang, C. Antony, F. Gunning, H. Zhang, and Y. L. Guan, "Discrete fresnel transform and its circular convolution," *unplubshed paper*, 2015. [Online]. Available: http://arxiv.org/abs/1510.00574

[58] V. Arrizón, J. G. Ibarra, and J. O.-C. neda, "Matrix formulation of the Fresnel transform of complex transmittance gratings," *Journal of the Optical Society of America A*, vol. 13, no. 12, pp. 2414–2422, Dec 1996.

# APPENDIX A – DISCRETE FRESNEL TRANSFORM

The DFnT, which was originated from the classical optics, is an integral transformation that mathematically describes the near-field optical diffraction [57, 58] and presents some interesting properties that allow its use in data communication systems through the OCDM scheme. Therefore, in this appendix is presented the DFnT matrix and some of its most valuable properties.

First of all, the DFnT is a square matrix and has different construction depending if the number of columns/rows is odd or even; however, in this thesis, only even values are considered. So, the elements of the $N \times N$-length DFnT matrix, $\mathbf{\Phi}$ is given by

$$\Phi_{m,n} = \frac{1}{\sqrt{N}} e^{-j\frac{\pi}{4}} e^{j\frac{\pi}{N}(m-n)^2}, \tag{A.1}$$

in which $m, n = 0, \ldots, N-1$. Therefore, the vector representation in the discrete-Fresnel domain, $\dot{\mathbf{z}} \in \mathbb{C}^{N\times 1}$, is given by

$$\dot{\mathbf{z}} = \mathbf{\Phi}\mathbf{z}, \tag{A.2}$$

in which $\mathbf{z} \in \mathbb{C}^{N\times 1}$ is a vector in another domain, which in this thesis cases is the discrete-time domain. And to bring back a vector from the discrete-Fresnel domain back to the original domain, it is necessary to apply the inverse discrete Fresnel transform (IDFnT), $\mathbf{\Phi}^\dagger$, as follows:

$$\mathbf{z} = \mathbf{\Phi}^\dagger \dot{\mathbf{z}}. \tag{A.3}$$

Note that the DFnT matrix is unitary, i.e. $\mathbf{\Phi}\mathbf{\Phi}^\dagger = \mathbf{\Phi}^\dagger\mathbf{\Phi} = \mathbf{I}_{2N}$. Moreover, the DFnT of a circular convolution is equal to the DFnT of either term convolving with the other [45]. To put in mathematical terms, the following expression applies:

$$\begin{aligned} \mathbf{\Phi r} &= \mathbf{\Phi B z} \\ &= \mathbf{B\Phi z}, \end{aligned} \tag{A.4}$$

where $\mathbf{r} = \mathbf{Bz}$ with $\mathbf{B} \in \mathbb{C}^{N\times N}$ being a circulant matrix and $\mathbf{z} \in \mathbb{C}^{N\times 1}$ is a vector.

Moreover, since the DFnT is a circulant matrix, the relation $\mathbf{F\Phi F}^\dagger$ will result in a diagonal matrix with inputs equal to the eigenvalue of $\mathbf{\Phi}$, in which

$$\mathbf{\Gamma} = \mathbf{F\Phi F}^\dagger. \tag{A.5}$$

Note (A.5) is very useful to simplify the equalization in the discrete-frequency domain, since one may rewrite (A.1) as $\mathbf{\Phi} = \mathbf{F}^\dagger\mathbf{\Gamma F}$, with $\mathbf{\Gamma}$ being a phase induced diagonal matrix with elements equal to

$$\Gamma_{k,k} = e^{-j\frac{\pi}{2N}k^2}, \tag{A.6}$$

which results in the receiver, $\dot{\mathbf{R}}$, is equal to

$$\begin{aligned} \dot{\mathbf{R}} &= \mathbf{\Phi F}^\dagger\mathbf{EF} \\ &= \mathbf{F}^\dagger\mathbf{\Gamma FF}^\dagger\mathbf{EF} \\ &= \mathbf{F}^\dagger\mathbf{\Gamma EF}. \end{aligned} \tag{A.7}$$

Also, since the DFnT is unitary, $\mathbf{\Gamma}$ is unitary as well. Finally, all the above expressions are valid for the type-IV version of the DFnT, as it is shown in [49].

# APPENDIX B – DISCRETE ORTHOGONAL STOCKWELL TRANSFORM - PARAMETERS

The OSDM scheme aims to allocate each symbol in an orthogonal tile that occupies a given frequency×time dimension that conforms to a $\mathcal{B}$-geometry. Each of these tiles are obtained following the DOST, given by (3.30), and characterized by the parameters $(\boldsymbol{\nu}, \boldsymbol{\beta}, \boldsymbol{\tau})$, which responsible for coordinating each tile to a given position in the time-frequency space. Also, each one of the mentioned parameters is build to assure baseband data communication [28].

A short descriptions of each of them are as follows:

- The first parameter, $\boldsymbol{\nu} \in \mathbb{N}^{2N\times 1}$, is related to the central frequency of the tile. And, it is given by the vector $\boldsymbol{\nu} = [\nu_0 \mathbf{1}_{\beta_0}^T, \nu_1 \mathbf{1}_{\beta_1}^T, \ldots, \nu_{N_p-1} \mathbf{1}_{\beta_{N_p-1}}^T]^T \in \mathbb{N}^{2N\times 1}$, where $N_p = 2\log_2(\mathcal{B}) + 2N/2$, $\mathbf{1}_{\beta_p}$ is a $\beta_p$-size column vector filled with ones, and $\nu_p$ is given by

$$\nu_p = \begin{cases} 0, & \text{for } p = 0 \\ 1, & \text{for } p = 1 \\ 2^{p-1} + 2^{p-2}, & \text{for } 2 \le p \le \log_2(\mathcal{B}) \\ \mathcal{B}(p - \log_2(\mathcal{B}) + 2^{-1}), & \text{for } \log_2(\mathcal{B}) + 1 \le p \le N_p/2 - 1 \\ 2N/2, & \text{for } p = N_p/2 \\ 2N + 1 - (N_p - \log_2(\mathcal{B}) + 2^{-1} - p)\mathcal{B}, & \text{for } N_p/2 + 1 \le p \le N_p - \log_2(\mathcal{B}) - 2 \\ -2^{-p-1+N_p} - 2^{-p-2+N_p} + 1 + 2N, & \text{for } N_p - \log_2(\mathcal{B}) - 1 \le p \le N_p - 2 \\ 2N - 1, & \text{for } p = N_p - 1. \end{cases} \tag{B.1}$$

  Different tiles sharing the same value of $\nu_k$ are called voice.

- The second parameter, $\boldsymbol{\beta} \in \mathbb{N}^{*2N\times 1}$, represents the tile's bandwidth. Therefore, it is given by the vector $\boldsymbol{\beta} = [\beta_0 \mathbf{1}_{\beta_0}^T, \beta_1 \mathbf{1}_{\beta_1}^T, \ldots, \beta_{N_p-1} \mathbf{1}_{\beta_{N_p-1}}^T]^T$, where $\beta_p$ is equal to

$$\beta_p = \begin{cases} 1, & \text{for } 0 \le p \le 1 \\ 2^{p-1}, & \text{for } 2 \le p \le \log_2(\mathcal{B}) \\ \mathcal{B}, & \text{for } \log_2(\mathcal{B}) + 1 \le p \le N_p/2 - 1 \\ 1, & \text{for } p = N_p/2 \\ \mathcal{B}, & \text{for } N_p/2 + 1 \le p \le N_p - \log_2(\mathcal{B}) - 2 \\ 2^{-p-1+N_p}, & \text{for } N_p - \log_2(\mathcal{B}) - 1 \le p \le N_p - 2 \\ 1, & \text{for } p = N_p - 1. \end{cases} \tag{B.2}$$

- The third parameter is represented by the vector $\boldsymbol{\tau} = [\mathbf{s}^T[0], \mathbf{s}^T[1], \ldots, \mathbf{s}^T[N_p - 1]]^T \in \mathbb{N}^{2N\times 1}$, where $\mathbf{s}[p]$ is given by

$$\mathbf{s}[p] = \begin{cases} [0], & \text{for } 0 \leq p \leq 1 \\ [0, \ldots, \beta_p - 1]^T, & \text{for } 2 \leq p < N_p/2 \\ [0], & \text{for } p = N_p/2 \\ [\beta_p - 1, \ldots, 0]^T, & \text{for } N_p/2 + 1 \leq p \leq N_p - 2 \\ [0], & \text{for } p = N_p - 1 \end{cases}, \tag{B.3}$$

  which is responsible for allocating a given tile in the time domain.

Figure 11 – Spectrogram of the OSDM scheme, while considering $N = 8$ and 2-geometry tiles.

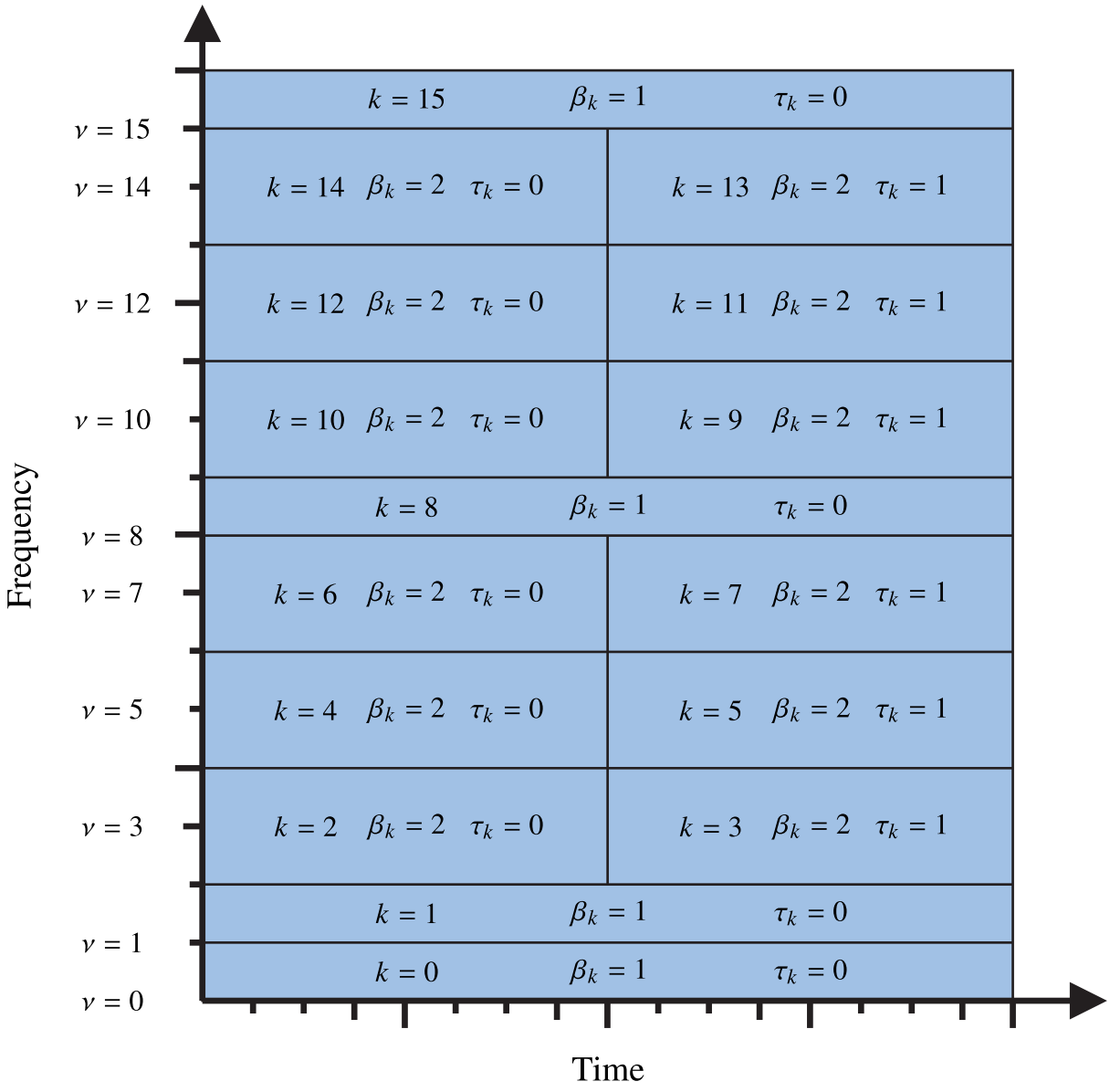

To help understand better how the three aforementioned parameters create the tile in which a signal is transmitted through. Figure 11 illustrates it when $2N = 16$ and $\mathcal{B} = 2$.

# APPENDIX C – PUBLICATIONS

The conference paper published during the graduate period is as follows:

- T. F. Moreira, Â. Camponogara, S. Baig, and M. V. Ribeiro, "Data rate and bit error probability in narrowband PLC systems: OCDM versus HS-OFDM," in *XXXIX Simpósio Brasileiro de Telecomunicações e Processamento de Sinais*, 2021, pp. 1–5.

The journal papers submitted during the graduate period are as follows:

- T. F. Moreira, Â. Camponogara, S. Baig, and M. V. Ribeiro, "Orthogonal chirp division multiplexing: New findings," *IEEE Access*, Jan. 2022. (submitted).
- Â. Camponogara, K. C. C. Santos, T. F. Moreira, and M. V. Ribeiro, "Secrecy in narrowband hybrid PLC/WLC systems under passive eavesdropping," *Wirel. Commun. Mob. Comput.*, Fev. 2022. (submitted)